Title: Blockade of EGFR improves responsiveness to PD1 blockade in *EGFR*-mutated non-small cell lung cancer

Authors: Eri Sugiyama,[1,2] Yosuke Togashi,[2] Yoshiko Takeuchi,[2] Sayoko Shinya,[2] Yasuko Tada,[2] Keisuke Kataoka,[3] Kenta Tane,[4] Eiichi Sato,[5] Genichiro Ishii,[6] Koichi Goto,[7] Yasushi Shintani,[8] Meinoshin Okumura,[8] Masahiro Tsuboi,[4] and Hiroyoshi Nishikawa[1,2*]

E.S. and Y. Togashi equally contributed to this work.

Affiliations:

[1]Department of Immunology, Nagoya University Graduate School of Medicine, Nagoya 466–8550, Japan.
[2]Division of Cancer Immunology, Research Institute/Exploratory Oncology Research & Clinical Trial Center (EPOC), National Cancer Center, Tokyo 104-0045/Chiba 277-8577, Japan.
[3]Division of Molecular Oncology, Research Institute, National Cancer Center, Tokyo 104-0045, Japan.
[5]Department of Pathology, Institute of Medical Science, Tokyo Medical University, 160-0023 Tokyo, Japan.
[4]Division of Thoracic Surgery, [6]Division of Pathology, [7]Division of Thoracic Oncology, National Cancer Center Hospital East, Chiba 277-8577, Japan.
[8]Department of General Thoracic Surgery, Osaka University Graduate School of Medicine, Osaka 565-0871, Japan.

***Corresponding authors:**
Hiroyoshi Nishikawa, MD, PhD,
Division of Cancer Immunology, Research Institute/EPOC, National Cancer Center,
6-5-1 Kashiwanoha, Kashiwa, Chiba 277-8577, Japan.
Phone: +81-4-7133-1111 (Ext. 2157/91385), Fax: +81-4-7130-0022
E-mail: hnishika@ncc.go.jp

One Sentence Summary: We propose a concept of immune-cell infiltration through the signals provided by driver gene alterations in the tumor.

Abstract:

The clinical efficacy of anti-PD-1 mAb against cancers with oncogenic driver gene mutations, which often harbor a low tumor mutation burden, is variable, suggesting different contributions of each driver mutation to immune responses. Here, we investigated the immunological phenotypes in the tumor microenvironment of *EGFR*-mutated lung adenocarcinomas, for which anti-PD-1 mAb is largely ineffective. While *EGFR*-mutated lung adenocarcinomas had a non-inflamed TME, $CD4^+$ effector regulatory T cells, which are generally present in the inflamed TME, showed high infiltration. The EGFR signal activated cJun/JNK and reduced IRF1; the former increased CCL22, which recruits $CD4^+$ effector regulatory T cells, and the latter decreased CXCL10 and CCL5, which induce $CD8^+$ T cell infiltration. EGFR inhibitor, erlotinib decreased $CD4^+$ effector regulatory T cells infiltration in the tumor microenvironment, and in combination with anti-PD-1 mAb showed better antitumor effects than either treatment alone. Our results suggest that EGFR inhibitors when used in conjunction with anti-PD-1 mAb could increase the efficacy of immunotherapy in lung adenocarcinomas.

Word counts: 6781 words (Abstract: 160 words)

Number of tables/figures: 5 figures, 16 supplementary figures and 7 supplementary tables.

[Main Text]

Introduction

Lung cancer, in which approximately 80% of cases are classified as non-small-cell lung cancer (NSCLC), is one of the leading causes of cancer-related mortality worldwide. Alterations in several oncogenic driver genes, including genes encoding epidermal growth factor receptor (*EGFR)* and anaplastic lymphoma kinase (*ALK),* have been reported in NSCLC. Molecular-targeted therapies directed against these driver gene alterations have been successfully developed, resulting in the improvement of patient prognosis (*1, 2*). The activating *EGFR* mutation is found in 50% of lung adenocarcinomas (LUADs) in East Asia, including Japan (*3*). While patients with *EGFR* mutations initially respond to EGFR-tyrosine kinase inhibitors, they usually become resistant to the therapy later. Thus, effective treatment strategies are urgently needed.

Recently, immune checkpoint blockade (ICB), including monoclonal antibodies (mAbs) against programmed cell death 1 (PD-1) and programmed cell death-ligand 1 (PD-L1), has demonstrated impressive antitumor effects in NSCLC, opening a new era in NSCLC treatment (*4, 5*). However, the efficacy is less than 50%, and development of treatments with increased efficacy is needed. Several approaches have been developed to augment the clinical efficacy of cancer immunotherapy, e.g., combination with

chemotherapy, anti-VEGF therapies, other ICBs, and regulatory T cell (Treg)-targeted therapies (*6*). Despite the promising results of ICB in NSCLC, a low clinical efficacy of anti-PD-1/PD-L1 mAbs against *EGFR*-mutated NSCLC has been reported. A retrospective study revealed that *EGFR*-mutated NSCLC has low expression rates of PD-L1, a predictive biomarker, and $CD8^+$ tumor-infiltrating lymphocytes (TILs) (*4, 7*). In contrast, other studies have shown that *EGFR*-mutated NSCLC cell lines have higher PD-L1 expression (*4, 5*) than *EGFR* wild-type NSCLC cell lines (*8, 9*).

Cancer cells with inherent genetic instability generate abnormal proteins, which have not been previously recognized by the immune system and become immunogenic antigens (neoantigens), thereby spontaneously triggering $CD8^+$ T cell responses that contribute to elimination of the cancer cells from the hosts (*10*). To avoid immune cell attack, cancer cells establish immune suppressive networks in the tumor microenvironment (TME), resulting in inflamed tumors characterized by concomitant infiltration of $CD8^+$ T cells and immune suppressive cells, such as Tregs and myeloid-derived suppressor cells (*6, 11*). However, poorly immunogenic cancer cells that are selected during cancer development harbor low levels of neoantigens derived from gene alterations, leading to non-inflamed tumors lacking both $CD8^+$ T cells and immune suppressive cells (*11*).

Cancers with oncogenic driver gene mutations, such as *EGFR* mutations, generally have a lower tumor mutation burden than cancers without these mutations, resulting in the development of a non-inflamed TME (e.g., low levels of $CD8^+$ T cells and immune suppressive cells) (*11, 12*). In this study, we explored the immunological status of the TME in *EGFR*-mutated lung adenocarcinomas (LUADs) and identified an intriguing immunological status: high Treg infiltration without $CD8^+$ T cell infiltration, which established a strong non-inflamed TME. The intense non-inflamed TME was attributed to the downstream signals of *EGFR* mutations that directly controlled T cell infiltration by changing the chemokine milieu in the TME. Therefore, researchers should develop optimal cancer immunotherapy based on the immune phenotypes in the TME.

Results

PD-L1 expression does not play an important role in preventing antitumor immune responses in EGFR-mutated LUADs

PD-L1 expression by tumor cells reduces effector T cell activity and promotes tumor progression (*13*). We first examined whether *EGFR*-mutated NSCLC cells possessed higher PD-L1 expression than *EGFR* wild-type NSCLC cells. Four cell lines (2 *EGFR*-mutated and 2 *EGFR* wild-type NSCLC cell lines) were prepared from regular cultures without any stimulation, such as cytokines, and *CD274* (encoding PD-L1) expression was examined. *CD274* expression was higher in the *EGFR*-mutated NSCLC cell lines than in the *EGFR* wild-type NSCLC cell lines (**Fig. S1**). To reflect the TME where tumor cells are exposed to interferon (IFN)-γ produced by T cells and other immune cells, we added IFN-γ to the cultures of these NSCLC cell lines. *CD274* expression was strongly elevated in both *EGFR*-mutated and *EGFR* wild-type NSCLC cell lines, resulting in comparable *CD274* expression levels (**Fig. S1**).

In addition, surgically resected tumor specimens from 19 patients with LUADs in which *EGFR* gene status had already been evaluated (6 *EGFR*-mutated and 13 *EGFR* wild-type LUADs) were subjected to RNAseq. *CD274* expression tended to be higher in *EGFR* wild-type LUAD than in *EGFR*-mutated LUAD, which was confirmed by IHC,

although the results were not significant (**Fig. 1A-C** and **Fig. S2**). A TCGA dataset also confirmed this trend (**Fig. S2**). Thus, high PD-L1 expression in *EGFR*-mutated NSCLC cell lines, which has been shown in several previous reports (*8*, *9*), did not reflect the TME in human NSCLCs and was not a major factor in raising antitumor immune responses in *EGFR*-mutated LUADs.

Immune-related gene expression and tumor mutation burden are decreased in EGFR-mutated LUADs

Nineteen LUAD samples subjected to RNAseq were clustered based on gene sets [$CD4^+$ Tregs, $CD8^+$ T cells, macrophages, dendritic cells, MHC class I, costimulatory antigen presenting cells (APCs) and T cells, coinhibitory APCs and T cells, IFN response, and cytolytic activity] (*11*); 6 samples were inflamed (i.e., high $CD8^+$ T cell genes and high cytolytic activity genes), and 13 samples were non-inflamed (**Fig. 1A**). Of 13 non-inflamed samples, 6 were *EGFR*-mutated LUADs, while all 6 inflamed samples were *EGFR* wild-type LUADs. *EGFR*-mutated LUADs showed substantially lower *CD274*, *PDCD1* (encoding PD-1), *CD8A*, *GZMA*, and *PRF1* expression than *EGFR* wild-type LUADs (**Fig. 1B** and **Fig. S2**). There was no significant difference in smoking status, stage, or tumor size between the inflamed and non-inflamed samples (**Fig. 1A**).

Next, whole exome sequencing was performed with LUAD samples from which sufficient DNA samples were available. Both nonsynonymous single nucleotide variants and frameshift mutations, which can reflect the number of gene alteration-associated neoantigens and are associated with clinical efficacy of anti-PD-1 mAbs (*10*), were significantly higher in *EGFR* wild-type LUADs than in *EGFR*-mutated LUADs (**Fig. 1D**). TCGA data also confirmed the higher immune-related gene expression and tumor mutation burden in *EGFR* wild-type LUADs than mutated LUADs (**Fig. S2**). These findings suggest that *EGFR*-mutated LUADs have a non-inflamed TME with a low tumor mutation burden.

Increased prevalence of Tregs in EGFR-mutated LUADs

In addition to gene assays of our 19 LUAD samples and TCGA data, flow cytometry and/or CyTOF assays with TILs collected from 26 surgically resected LUADs (7 *EGFR*-mutated and 19 *EGFR* wild-type LUADs) were performed for detailed immune profiling of the TME. In *EGFR*-mutated LUADs, the frequency of $CD8^+$ T cells was lower than that of the *EGFR* wild-type LUADs in CyTOF, consistent with the RNAseq results. Additionally, activated PD-1^+CD8^+ T cell and $Gzmb^+CD8^+$ T cell fractions were reduced in *EGFR*-mutated LUADs (**Fig. 2A** and **Fig. S3**). Importantly, $FOXP3^+CD4^+$ Tregs,

which are generally accompanied by effector T cells such as $CD8^+$ T cells (*14*), were highly detected in *EGFR*-mutated LUADs (**Fig. 2A**).

To validate these data, we also investigated TILs with flow cytometry. Correct identification of Tregs in humans is compromised due to the upregulation of FOXP3 upon TCR stimulation in conventional T cells (*15*). We have therefore proposed a classification of human Tregs based on the expression levels of a naive marker CD45RA and FOXP3, and $FOXP3^+CD4^+$ T cells can be divided into three fractions: naive Tregs (Fr. I: nTregs, $CD45RA^+FOXP3^{low}CD4^+$); effector Tregs (Fr. II: eTregs, $CD45RA^-FOXP3^{high}CD4^+$) with strong immune suppressive functions; and non-Tregs (Fr. III: $CD45RA^-$ $FOXP3^{low}CD4^+$) without suppressive functions (**Fig. 2B**) (*16-18*). TIL analyses with flow cytometry confirmed that the frequency of $CD8^+$ T cells tended to be lower in *EGFR*-mutated LUADs than in *EGFR* wild-type LUADs (**Fig. 2B**). The frequency of tumor-infiltrating eTregs and the eTreg/$CD8^+$ T cell ratio were significantly higher in *EGFR*-mutated LUADs than in *EGFR* wild-type LUADs, corresponding to the data from CyTOF and IHC (**Fig. 1C**, **2A**, and **2B)**. These findings suggest that Tregs infiltrate into the TME despite the low levels of $CD8^+$ effector T cells in *EGFR*-mutated LUADs. In contrast, only 2 of 19 patients with *EGFR* wild-type LUADs (AD #15 and #16) had a high eTreg/$CD8^+$ T cell ratio (> 0.2) (**Fig. 2B**), and *FOXP3* expression in these patients was

very high in accordance with the inflamed TME (**Fig. 1A** and **Fig. S2**). Such patients seemed to have "inflammation-related acquired Tregs" in the TME, and indeed, the FOXP3 gene, a representative Treg-related gene, was clustered into inflamed gene sets (*14*) (**Fig. 1A** and **Fig. S4A**). There was no significant correlation between smoking status, stage, or tumor size and $CD8^+$ T cell or eTreg infiltration (**Fig. S5**).

In addition to Treg infiltration, tumor-associated macrophages (TAMs: $CD68^+CD163^+CD206^+$ cells), myeloid-derived suppressor cells (MDSCs: $CD33^+CD11b^+$ cells) and dendritic cells (DCs: $CD11c^+CD11b^-$HLA-DR^+ cells) were analyzed with multiplex fluorescent IHC. In *EGFR*-mutated LUADs, the frequencies of TAMs, MDSCs and DCs tended to be slightly, but not significantly, higher, than those of *EGFR* wild-type LUADs, which is consistent with the RNAseq data (**Fig. 1A** and **Fig. S6**).

Chemokine changes by EGFR signals are associated with the immune phenotypes in EGFR-mutated LUADs

To gain insight into the mechanism(s) for this immunological status of *EGFR*-mutated LUADs (high Treg infiltration despite low $CD8^+$ effector T-cell infiltration), we investigated the effect of EGFR signaling on $CD8^+$ effector T cells and Treg infiltration with two *EGFR*-mutated cell lines (PC-9 and HCC827) and an *EGFR* wild-type cell line

(H322) treated with erlotinib and EGF, respectively. Comprehensive gene expression was analyzed with a microarray, and gene set enrichment analysis (GSEA) revealed that the gene signature of INTERFERON_GAMMA_RESPONSE, which is associated with chemokine (CXCL10 and CCL5) production, was commonly enriched in the downregulated state of the EGFR signal (**Fig. S7**). Consistently, we found that GO terms, cytokines and chemokines, such as *CCL5* and *CXCL10*, which reportedly recruit $CD8^+$ T cells (*19, 20*), were downregulated by EGFR signaling (**Fig. 3A**). Additionally, *CCL22*, which recruits Tregs (*18, 21, 22*), was elevated with activation of EGFR signaling (*EGFR*-mutated cell lines without erlotinib and *EGFR* wild-type cell line with EGF) (**Fig. 3A**). This elevation was abrogated by inhibition of EGFR signaling with an erlotinib in *EGFR*-mutated cell lines. The changes in mRNA and protein expression were observed with both erlotinib and third-generation EGFR-tyrosine kinase inhibitor (osimertinib), as shown by qRT-PCR and by ELISAs (**Fig. 3B**, **3C**, **Fig. S8** and **S9**).

EGFR signaling controls the transcription factors cJun/JNK and IRF1 for the immune phenotype of EGFR-mutated LUADs

To further examine chemokine changes by EGFR signaling, we examined the transcriptional regulation of these chemokines. Since the *JNK/cJun* pathway has been

reported to increase *CCL22* expression (*23*), *JUN* expression was examined. *JUN* expression was augmented along with *CCL22* expression (**Fig. 4A** and **B**). The increases in cJUN and phospho-cJUN were induced by pJNK via EGFR signaling (**Fig. 4C**). In addition, *JUN* knockdown decreased *CCL22* expression but not *CXCL10* expression (**Fig. 4D**). A luciferase assay using *CCL22* promoter regions also demonstrated that *JUN* knockdown decreased *CCL22* luciferase activity (**Fig. 4D**), suggesting that EGFR signaling increases *CCL22* expression via *JNK/cJun* activation.

To investigate the mechanism(s) of *CCL5* and *CXCL10* reduction, we examined a transcription factor(s) that showed comparable changes to *CXCL10* in the microarray data. We found that *IRF1* expression was concurrently changed with *CXCL10* expression (**Fig. 4A**) and was downregulated by the activation of EGFR signaling (**Fig. 4A** and **B**). The PI3K/AKT pathway, which is downstream of the EGFR signal, has been reported to inhibit IRF1 expression (*24, 25*). Accordingly, pAKT was increased by the activation of the EGFR signal, consequently decreasing IRF1 (**Fig. 4C**). Additionally, *IRF1* knockdown resulted in the downregulation of *CXCL10,* but not *CCL22*, at the mRNA level and in luciferase assays (**Fig. 4E**), indicating that the EGFR signaling decreased *CXCL10* expression via *IRF1* inhibition. We propose the EGFR signaling plays an important role in driving high Treg infiltration despite low $CD8^+$ effector T-cell

infiltration in *EGFR*-mutated LUADs via *CCL22* upregulation through *JNK/cJun* and *CXCL10* downregulation mediated by *IRF1* (**Fig. S4B**).

A combination with erlotinib and anti-PD-1 mAb is a potential treatment strategy for EGFR-mutated LUADs

The functions of immune cells expressing EGFR might be directly modified the by EGFR tyrosine kinase inhibitor (*26, 27*). To evaluate the direct effect of erlotinib on $CD8^+$ T cells and Tregs, we analyzed EGFR expression by immune cells in PBMC and their sensitivity to erlotinib. Immune cells, including $CD8^+$ T cells and Tregs, possessed limited expression of EGFR compared with lung cancer cell line PC-9 (**Fig. S10A**). Accordingly, both $CD8^+$ T cells and Tregs failed to respond to erlotinib treatment (**Fig. S10B** and **C**). In addition, phospho-JAK2 and phospho-STAT5, which are downstream of the EGFR signal in immune cells (*28*) was not altered, and the expression levels of chemokines (*CXCL10*, *CCL5*, and *CCL22*) and transcription factors (*IRF1* and *JUN*) were not changed (**Fig. S10D** and **E**). These findings indicate that the EGFR signal does not directly influence on $CD8^+$ T cells and Tregs.

We next addressed whether EGFR signal inhibition altered the immunological

status (high Treg infiltration despite low $CD8^+$ effector T cell infiltration) of *EGFR*-mutated LUADs and prevented tumor growth/progression. Treg frequency in the TME of patients with *EGFR*-mutated LUADs who received erlotinib treatment was examined. Treg infiltration was significantly reduced after erlotinib treatment (**Fig. 5A**), suggesting that a combination treatment with erlotinib and anti-PD-1 mAb could be possible. *CXCL10* expression tended to be higher and *CCL22* expression tended to be lower after erlotinib treatment than before erlotinib treatment in patients with *EGFR*-mutated LUADs, although there was no significant difference due to the small size of our patient cohort (**Fig. S11**).

We then employed human *EGFR* mutant (exon 19 deletion)-transfected mouse cell lines, a bulk cell line after transfection and 2 single clones of MC-38ex19del, to examine the *in vivo* antitumor activity (**Fig. 5B, S12A** and **S13**). Compared with those of *EGFR* wild-type transfected cell line (MC-38wt)-derived tumors, higher and lower frequencies of Tregs and $CD8^+$ T cells, respectively, were observed in the TME of MC-38ex19del-derived tumors. The high Treg and low $CD8^+$ T-cell infiltration in the TME was totally abrogated by erlotinib treatment (**Fig. 5C**). In addition, consistent changes in chemokines and transcription factors were observed: *CXCL10*, *CCL5* and *IRF1* were downregulated in MC-38ex19del-derived tumors and were increased by erlotinib

treatment. *CCL22* and *JUN* were upregulated in MC-38ex19del-derived tumors and were reduced by erlotinib treatment (**Fig. 5D**). Furthermore, when CXCL10 was blocked with an antibody, the elevation of $CD8^+$ T cells in the TME induced by erlotinib treatment was abrogated (**Fig. S14A**), and no synergistic effect of erlotinib and anti-CCL22 mAb on Tregs in the TME was observed (**Fig. S14B**). Consequently, the combination of erlotinib and anti-PD-1 mAb significantly inhibited tumor growth compared with the control or either single treatment using a bulk cell line after transfection and 2 single clones of MC-38ex19del (**Fig. 5E** and **S12B**). In contrast, no synergistic effect of erlotinib and anti-PD-1 mAbs was observed in the control cell lines (MC-38mock and MC-38wt) (**Fig. 5E**). Moreover, this combination treatment exhibited a superior antitumor effect on orthotopic *EGFR* exon 19 deletion-transfected LL/2 (LL/2ex19del: a bulk cell line after transfection) than either treatment alone (**Fig. 5F** and **G**). Additional Treg depletion with anti-CD25 mAb failed to show any synergistic or additive antitumor effects (**Fig. S15**). Our results suggest that combination treatment with EGFR tyrosine kinase inhibitor such as erlotinib and anti-PD-1 can be a promising strategy for the treatment of *EGFR*-mutated LUADs.

Discussion

Cancers are immunologically divided into two major types, inflamed and non-inflamed tumors. Tregs have been thought to be recruited by inflammation into the TME ("inflammation-related acquired Treg") (**Fig. S4**) (*14*), as was observed in *EGFR* wild-type LUADs. In this study, we identified an intriguing immunological status in *EGFR*-mutated LUADs: high Treg infiltration despite the non-inflamed TME. We then proposed a concept of immune suppression, particularly by Tregs in the TME, "tumor-related innate Tregs" (**Fig. S4**). The dependence of tumor growth and/or survival on driver gene alterations such as *EGFR* mutations or *ALK* rearrangements in NSCLC is known as oncogenic driver addiction. Patients with such oncogenic driver gene alterations respond to molecular-targeted therapies (*1, 2*), indicating an important role of such oncogenic driver gene alterations in cell growth or survival. Additionally, we found that these gene alterations play another crucial role in immune responses through development of an immune suppressive environment in the TME of *EGFR*-mutated LUADs. Together, driver genes contribute to not only cell growth and/or survival but also immune escape from antitumor immunity.

Several previous studies have demonstrated that *EGFR*-mutated NSCLC cell lines have higher expression of PD-L1, one of the predictive biomarkers of PD-1/PD-L1

blockade therapies (*5*), than *EGFR* wild-type NSCLC cell lines (*8, 9*). PD-L1 expression is induced by two different mechanisms: genetic alterations (i.e., amplification, fusion and 3'UTR disruption) (innate expression) and induction by inflammation (such as acquired IFN-γ expression) (*13*). We revealed that while *EGFR*-mutated NSCLC cell lines cultured with regular medium without any stimulation, such as cytokines, exhibited slightly higher *CD274* (encoding PD-L1) expression than *EGFR* wild-type NSCLC cell lines, *CD274* expression was strongly enhanced by IFN-γ, showing a strong elevation of *CD274* expression in both *EGFR*-mutated and *EGFR* wild-type NSCLC cell lines regardless of their original expression. Interestingly, the extent of *CD274* elevation induced by IFN-γ was significantly higher in *EGFR* wild-type NSCLC cell lines than in *EGFR*-mutated NSCLC cell lines. *CD274* expression is primarily regulated by IFN-γ via *IRF1* (*29*), and our study revealed that EGFR signaling negatively regulated *IRF1*. Therefore, *IRF1* is suppressed by EGFR signaling in *EGFR*-mutated LUADs, resulting in a low increase in *CD274* expression by IFN-γ. Indeed, RNAseq and IHC exhibited higher PD-L1 expression in *EGFR* wild-type LUADs than in *EGFR*-mutated LUADs, and PD-1 blockade resulted in poor clinical responses in *EGFR*-mutated LUADs (*4, 7, 30*).

The clinical responses of anti-PD-1/PD-L1 mAbs against *EGFR*-mutated LUADs

were unfavorable due to the low tumor mutation burden, low PD-L1 expression, and the non-inflamed TME (*7, 30*). Tumor mutation burden can be reflected in the number of neoantigens derived from gene alterations, which induce a strong immune response as nonself antigens, leading to an inflamed TME. Thus, tumor mutation burden is reportedly associated with the clinical efficacy of anti-PD-1/PD-L1 mAbs (*10*). In our analyses, as tumor mutation burden was low in *EGFR*-mutated LUADs, immune-related gene expression was low in *EGFR*-mutated LUADs. Treg infiltration, which was frequently accompanied by $CD8^+$ T-cell infiltration in the inflamed TME (*14*), in *EGFR*-mutated cancers tended to be higher or comparable with that in *EGFR* wild-type cancers, although $CD8^+$ T-cell infiltration was limited in *EGFR*-mutated cancers. Therefore, the TME (high Treg infiltration without $CD8^+$ T-cell infiltration) was not developed solely due to low tumor mutation burden; rather, the immunological effects of *EGFR* mutations must be strongly involved via prevention of the recruitment of effector $CD8^+$ T cells by downregulation of *CXCL10* through *IRF1* and promotion of Treg infiltration by upregulation of *CCL22* through *cJun/JNK*. Considering that Tregs hamper the development of effective antitumor immunity in tumor-bearing hosts (*18*), the immunological status in the TME induced by *EGFR* mutations can be associated with resistance to cancer immunotherapy, as observed in our *in vivo* study, suggesting that

combination treatment of anti-PD-1 mAb and EGFR signal inhibitors should augment the antitumor efficacy. Indeed, in patients with advanced *EGFR*-mutated LUADs, tumor-infiltrating eTreg frequency was significantly lower after erlotinib treatment. While several clinical trials of erlotinib in combination with anti-PD-1 mAb have been performed, the high incidence of treatment-related adverse effects limited successful clinical application. In contrast, a recent phase III trial demonstrated that anti-PD-L1 antibody combined with bevacizumab, an anti-VEGF therapy, exhibits clinical efficacy against *EGFR*-mutated NSCLC (*31*). Antiangiogenic drugs reportedly reduced Tregs (*32*), which can partially explain the superior clinical efficacy of the combination therapy against *EGFR*-mutated NSCLC. However, the tumor mutation burden is lower in *EGFR*-mutated NSCLC than in *EGFR* wild-type NSCLC, indicating smaller numbers of neoantigens. In addition to regulating EGFR signaling, combination strategies that elicit $CD8^+$ T cells against cancer antigens, although the number is limited, may provide notably favorable clinical efficacy in *EGFR*-mutated NSCLC.

Chemokine production is controlled by multiple components, such as tumor cells and immune cells (*33*). Consistent with this finding, the basal level of CCL22 production in the *EGFR* wild-type H322 cell line was higher than in other *EGFR*-mutated cell lines. Inflammatory signals provided in the TME may imprint CCL22 production in the H322

cell line. Therefore, while *CCL22* expression is regulated by the cJUN/JNK signal, which is downstream of the EGFR signal in our data, many other signals may regulate CCL22 expression (*34*). Thus, tumor cell line information may not directly influence the TME. In MC-38 tumor model in which we can directly examine the role of EGFR signaling in *CCL22* expression, MC-38 with an *EGFR* mutation clearly increased *CCL22* expression compared with wild-type MC-38, resulting in enhanced Treg infiltration in the TME. These findings indicated the critical roles of chemokines derived from *EGFR*-mutated cancers in both Treg and $CD8^+$ T cell infiltration in the TME. The other chemokines that showed elevation with EGFR signal activation was *CXCL8,* which reportedly mainly recruited neutrophils (*35*). In contrast, *CCL21* (a ligand of CCR7), which mainly promoted the chemotaxis of natural killer T cells and naive T cells (*36*), respectively, were downregulated by the EGFR signals, consistent with the non-inflamed TME in *EGFR*-mutated cancer (**Fig. S16**). However, consistent tendencies were not observed in the RNAseq data.

While EGFR expression by immune cells, including Tregs, has been detected (*26, 27*), we found limited expression of EGFR in Tregs and $CD8^+$ T cells. Accordingly, erlotinib treatment did not influence the viability or function, including chemokines, of these cells. In addition, synergistic antitumor effects by the combination of erlotinib and

anti-PD-1 mAb in EGFR wild-type cancers were not observed when compared with that of anti-PD-1 mAb alone. As EGFR expression by Tregs was reported in inflammatory conditions (*26*), one plausible explanation is that immune cells, particularly Tregs, employ various different signals for molecular expression depending on each condition, such as cancers and inflammation. In *EGFR*-mutated cancers, the non-inflamed immune suppressive TME (high Tregs and low $CD8^+$ T cells) may reduce the expression of EGFR by immune cells such as Tregs.

In conclusion, we found an intriguing immunological status in the TME of *EGFR*-mutated LUADs: high Treg infiltration despite the non-inflamed TME. Tregs are primarily recruited via signals from tumor cells ("tumor-related innate Tregs"), which are induced by driver gene alterations such as *EGFR* mutations and related to resistance to cancer immunotherapies. Driver gene alterations represented by *EGFR* mutations therefore play an important role in cell growth and/or survival as well as the development of immune escape machineries, warranting further tests in cancer immunotherapies combined with molecular-targeted therapies against cancers with driver gene alterations.

Materials and Methods

Patients and samples

Peripheral blood and tumor tissues were obtained from patients with LUADs who underwent surgery at Osaka University Hospital and National Cancer Center Hospital East from 2014 to 2015 and advanced LUAD patients harboring *EGFR* mutations who received EGFR-tyrosine kinase inhibitors, such as gefitinib, erlotinib and afatinib, treatment at National Cancer Center Hospital East from 2015 to 2016 (summarized in **Table S1** and **S2**, respectively). Peripheral blood mononuclear cells (PBMCs) were isolated by density gradient centrifugation with Ficoll-Paque (GE Healthcare, Little Chalfont, UK). For collection of TILs, tumor tissues were minced and treated with gentleMACS Dissociator (Miltenyi Biotec, Bergisch Gladbach, Germany) as described previously (*17*). PBMCs from healthy individuals were purchased from Cellular Technology Limited (Cleveland, OH). PBMCs were cultured in RPMI 1640 supplemented with 10% AB serum. PBMCs were cultured with CD3/CD28 Dynabeads (Thermo Fisher Scientific, Waltham, MA) according to the manufacturer's instructions for 3 days. All donors provided written informed consent before sampling, according to the Declaration of Helsinki. This study was performed in a blinded and nonrandomized manner and was approved by Osaka University Hospital Ethics Committee and National

Cancer Center Ethics Committee.

Immunohistochemistry (IHC) for PD-L1, CD8, and FOXP3

The antibodies used in IHC are summarized in **Table S3**. Surgically resected samples were formalin-fixed, paraffin-embedded, and sectioned onto slides for IHC. The slides were deparaffinized with xylene, rehydrated, and antigen-retrieved in a microwave oven for 20 minutes. After the inhibition of endogenous peroxidase activity, individual slides were then incubated overnight at 4°C with a mouse anti-human CD8 mAb, a rabbit anti-human FOXP3 mAb, and a rabbit anti-human PD-L1 mAb. The slides were then incubated with EnVision reagent (Dako, Glostrup, Denmark), and a color reaction was developed in 2% 3,3-diaminobenzidine in 50 mM Tris buffer (pH 7.6) containing 0.3% hydrogen peroxidase. Finally, these sections were counterstained with Meyer hematoxylin. PD-L1 positivity was evaluated in the tumor cells. CD8 and FOXP3 staining was quantified in five high-power microscopic fields (x400; 0.0625 mm^2) and the mean values were calculated. Two pathological researchers (E.S. and G.I.) independently evaluated the stained slides.

Multiplex immunofluorescence staining

The antibodies used in multiplex immunofluorescence staining are also described in **Table S3**. Surgically resected samples were formalin-fixed, paraffin-embedded, and sectioned onto slides. The slides were deparaffinized with xylene, rehydrated, and antigen-retrieved in a microwave oven for 40 minutes. After the inhibition of endogenous peroxidase activity, individual slides were then incubated for 1 hour at room temperature with a rabbit anti-human CD33 mAb, a rabbit anti-human CD11b mAb, a rabbit anti-human CD11c mAb, a mouse anti-human CD68 mAb, a mouse anti-human CD163 mAb, a mouse anti-human CD206 mAb, and a rabbit anti-human HLA-DR mAb. Anti-rabbit/mouse polymeric horseradish peroxidase (System-HRP labeled polymer anti-rabbit, Envision, Dako) was applied as the secondary label for 20 minutes. Signals from the antibody complexes were visualized with their corresponding Opal Fluorophore Reagents (PerkinElmer, Waltham, MA) after incubation of the slides for 10 minutes. Slides were air dried, mounted with ProLong Diamond Antifade mounting medium (Thermo Fisher) and stored in a light-proof box at 4°C before imaging. Multiplexed fluorescent labeled images of one to five randomly selected fields (669×500 micrometer) were captured with an automated imaging system (Vectra 3, PerkinElmer). Cell counts were determined manually for each image.

CyTOF analysis

CyTOF staining and analysis were performed as described (*37*). The antibodies used in the CyTOF analyses are summarized in **Table S4**. Cells were subjected to staining after they were washed with PBS supplemented with 2% FCS (washing solution) and then with PBS to reduce the protein concentration in the medium, which interferes with the subsequent dead cell staining by cisplatin. The cells were incubated in 5 μM of Cell-ID Cisplatin solution (Fluidigm Cat#201064, South San Francisco, CA) in PBS, washed using washing solution, and stained with a mixture of surface antibodies. After the cells were washed, they were fixed and permeabilized using Foxp3/Transcription Factor Staining Buffer Set (Thermo Fisher Scientific Cat#00-5523-00) according to the manufacturer's instructions. The fixed and permeabilized cells were then stained with the intracellular antibodies. After the cells were washed twice, they were rested overnight in 125 nM MaxPar Intercalator-Ir (Fluidigm Cat#201192B) diluted in 2% paraformaldehyde PBS solution at 4°C. The cells were then washed once with washing solution and twice with MaxPar water (Fluidigm Cat#201069), distilled water with minimal heavy element contamination, to reduce the background level. The cells suspended in MaxPar water supplemented with 10% EQ Four Element Calibration Beads (Fluidigm Cat#201078) were applied to the Helios instrument (Fluidigm), and data were acquired at a speed below

300 events/second.

Flow cytometry analysis

Flow cytometry staining and analysis were performed as described (*37*). The antibodies used in the flow cytometry analyses are summarized in **Table S5**. Cells were washed using washing solution and subjected to staining with surface antibodies. Intracellular staining of FOXP3, pJAK2 and pSTAT5 was performed with anti-Foxp3 mAb, anti-pJAK2 mAb and anti-pSTAT5 mAb and the Foxp3/Transcription Factor Staining Buffer Set (Thermo Fisher Scientific) according to the manufacturer's instructions. After the cells were washed, they were analyzed with an LSRFortessa or FACSymphony (BD Biosciences, Franklin Lakes, NJ) and FlowJo software (Treestar, Ashland, OR). The staining antibodies were diluted according to the manufacturer's instructions.

RNAseq

After quality assessment with an Agilent 2100 Bioanalyzer (Agilent Technologies, Santa Clara, CA), polyadenylated RNA libraries were generated using a Truseq Stranded mRNA Sample Prep Kit (Illumina, San Diego, CA) on an Agilent XT-Auto System (Agilent Technologies) and sequenced with a HiSeq SBS Kit v4-HS (Illumina) on

HiSeq2500 (Illumina). Sequence data were evaluated with GeneData Expressionist for Genomic Profiling (version 9.1.4a). Read-mapping was performed with Hg19 as the reference genome and TopHat (version 2.0.14), followed by transcriptome reconstruction and expression quantification into FPKM.

Whole-exome sequencing and mutational analysis

DNA libraries were established with a SureSelect XT Human All Exon system (Agilent Technologies) and sequenced with a HiSeq SBS Kit v4-HS (Illumina) on a HiSeq2500 system (Illumina) to generate paired-end reads (2 x 100 bp). Sequence alignment and mutation calling were performed using the Genomon pipeline (https://github.com/Genomon-Project/), as described previously (*38*). Candidate mutations were detected by the Empirical Bayesian Mutation Calling (EBCall) algorithm, and those with (i) a P value $< 10^{-4}$; (ii) > 4 variant reads in tumor samples; and (iii) a VAF value in tumor samples of > 0.025 were adopted. These candidate mutations were further filtered by excluding (i) synonymous single nucleotide variants (SNVs); (ii) known variants listed in the 1000 Genomes Project (October 2014 release), NCBI dbSNP build 131, National Heart, Lung, and Blood Institute (NHLBI) Exome Sequencing Project

(ESP) 6500, Human Genome Variation Database (HGVD) or our in-house SNP database; and (iii) variants present only in unidirectional reads.

Gene expression data analysis

In addition to our RNAseq dataset, The Cancer Genome Atlas (TCGA) dataset of LUADs was also analyzed. The *EGFR* gene status and mutation burden for 230 LUADs were evaluated based on previously published reports, and gene expression profiles and nonsynonymous mutations of these samples were extracted from the TCGA data portal (https://tcga-data.nci.nih.gov/tcga/tcgaHome2.jsp). For clustering, we used Cluster 3 for $CD4^+$ Treg, $CD8^+$ T cell, macrophage, dendritic cell, MHC class I cell, costimulatory APC and T cell, coinhibitory APC and T cell, type I IFN response, type II IFN response, and cytolytic activity gene sets as previously reported (*11*).

GSEA

GSEA was carried out to analyze the differences between two groups: activated EGFR signaling and inhibited EGFR signaling in three lung cancer cell lines (PC-9, HCC827 and H322). The gene sets were adopted from The Molecular Signatures Database. The phenotype label was EGFR activation score vs. EGFR inhibition score.

Gene expression analysis using the nCounter platform

For RNA purification, 10 μm FFPE slides were used for each tumor specimen. RNA was extracted using the RecoverAll™ Total Nucleic Acid Isolation Kit (Thermo Fisher Scientific). A minimum of 100 ng of total RNA was used to measure chemokine expression. Gene expression analyses were performed using the Human PanCancer IO 360 Panel and nCounter Low RNA Input Kit (Nanostring Technologies, Seattle, WA). Data were normalized by nSolver analysis software.

Cell line and reagents

A549, H322 and HCC827 cells (human NSCLC cell lines) were obtained from ATCC (Manassas, VA) (ATCC Cat#CRL-7909, Cat#CRL-5806, and Cat#CRL-2868, respectively), and PC-9 cell line (human NSCLC cell line) was obtained from ECACC (Salisbury, UK) (ECACC Cat#90071810). MC-38 cell line (mouse colon cancer cell line) was obtained from Kerafast (Boston, MA) (Cat#ENH204), and LL/2 cell line (mouse lung cancer cell line) was obtained from ATCC (ATCC Cat#CRL-1642). All human cell lines were authenticated using a short tandem repeat DNA method. The A549 and LL/2 cell lines were maintained in DMEM medium (Fujifilm Wako Pure Chemical Corporation,

Osaka, Japan) supplemented with 10% FCS. The H322, HCC827 and MC-38 cell lines were maintained in RPMI medium (Fujifilm Wako Pure Chemical Corporation) supplemented with 10% FCS. The human *EGFR* (wild-type or exon 19 deletion)-overexpressing MC-38 and LL/2 cell lines were established retrovirally using a pBabe-puro vector (Addgene Cat#1764, Cambridge, MA) (named MC-38wt, MC-38ex19del, LL/2wt, and LL/2ex19del cell lines). Erlotinib (Cat#10483) was obtained from Cayman Chemical Company (Ann Arbor, MI), osimertinib was purchased from Selleck (Houston, TX), anti-mouse PD-1 mAb was kindly provided by Ono Pharmaceutical (Osaka, Japan), anti-mouse CXCL10 mAb (clone 134013, Cat# MAB466-100) and anti-mouse CCL22 mAb (clone 158132, Cat# AF439) were obtained from R&D Systems (Minneapolis, MN), and anti-mouse CD25 (clone PC61, Cat#102040) was purchased from Biolegend (San Diego, CA). IFN-γ and EGF were purchased from Peprotech (Rocky Hill, NJ).

Quantitative real-time reverse transcription-PCR (qRT-PCR) and microarray analyses

Total RNA was reverse transcribed to cDNA using a SuperScript VILO Master Mix according to the manufacturer's instructions (Thermo Fisher Scientific), and real-time PCR was performed with PowerUp SYBR (Thermo Fisher Scientific). The GAPDH gene was used as an endogenous control, and the primers used are summarized in **Table S6**.

Microarray analysis was performed using the Clariom S array according to the manufacturer's instructions (Thermo Fisher Scientific).

ELISA

The concentrations of CXCL10 and CCL22 were examined with a specific sandwich ELISA according to the manufacturer's instructions (R&D Systems Cat#DMD00 and Cat#DIP100).

Western blotting

Subconfluent cells were washed with PBS and harvested with M-PER (Thermo Fisher Scientific). Whole-cell lyses were separated with SDS-PAGE and were blotted onto a polyvinylidene fluoride membrane. After the membrane was blocked, it was probed with the primary antibody. After the membrane was rinsed twice with TBS buffer, it was incubated with a horseradish peroxidase-conjugated secondary antibody and washed, followed by visualization using an ECL detection system and a LAS-4000 (GE Healthcare). The antibodies used in western blot analyses are summarized in **Table S7**.

siRNA

Cells were transfected with a siRNA for *JUN* or *IRF1* and a nonspecific target (control) using RNAiMAX (Thermo Fisher Scientific). ON-TARGETplus Human *JUN* siRNA SMART pool (Dharmacon Cat#L-003268-00-0005, Lafayette, CO), ON-TARGETplus Human *IRF1* siRNA SMART pool (Dharmacon Cat#L-011704-00-0005), and ON-TARGETplus Non-targeting Pool (Dharmacon Cat#D-001810-1005) were used.

Luciferase assay

A pNL2.1 vector (Promega Cat#N1061, Madison, WI) containing the *CXCL10* or *CCL22* promoter region upstream of the luciferase gene was generated. Luciferase activity was determined using the Luciferase Assay System (Promega Cat#N1110). The results are reported as the fold induction compared with the control group.

In vivo animal model

C57BL/6 mice (6-week-old females; CLEA Japan, Tokyo, Japan) were used for the *in vivo* studies. Animal care and experiments were conducted according to the guidelines established by the animal committee of the National Cancer Center after approval of the Ethics Review Committee for Animal Experimentation of the National Cancer Center. A suspension of 1×10^6 transfected cells (in 100 μL of PBS) was subcutaneously (MC-38)

or intravenously (LL/2) administered, and treatment was started after one week, when tumors in each group reached an average volume of approximately 500 mm^3. In some groups, anti-PD-1 mAb (obtained from Ono Pharmaceutical; 200 μg/body, i.p.) was administered at one-week intervals with or without oral daily erlotinib (obtained from Cayman Chemical Company, MI; 30 mg/kg) for 3 weeks. The tumor volume was assessed twice a week as the length × $width^2$ × 0.5. For blocking of CXCL10 and CCL22, 50 μg of anti-mouse CXCL10 mAb and 20 μg of anti-mouse CCL22 mAb, respectively, were administered intraperitoneally on days 4 and 7 after tumor implantation. For depletion of Tregs, 200 μg of anti-mouse CD25 mAb was administered intraperitoneally on day 7 after tumor implantation. TIL analysis was performed on day 10.

WST1 assay

The WST1 assay was performed according to the manufacturer's instructions to evaluate the sensitivities to erlotinib and cell proliferation. After each cell line was seeded in a 96-well plate, the cells were incubated with erlotinib for 48 hours. Then, WST1 reagent (10% of medium) was added, and absorbance was analyzed by a microplate reader at 450 nm and 690 nm. The proliferation of the transfected MC-38 cell lines was analyzed in the same way without erlotinib 0, 24 and 48 hours after seeding.

Statistical analysis

Continuous variables were analyzed with Welch's or paired t-tests. Survival curves were estimated with the Kaplan–Meier method and compared with the log-rank test. The statistical analyses were performed with Prism version 7 software (GraphPad Software, Inc., La Jolla, CA). A *P*-value of less than 0.05 was considered statistically significant.

List of Supplementary Materials

Figure S1. Comparable *CD274* expression between *EGFR*-mutated and *EGFR* wild-type NSCLC cell lines after IFN-γ treatment.

Figure S2. The expression of *CD274* and other immune-related genes and tumor mutation burden in *EGFR*-mutated and wild-type LUADs in our cohort and TCGA data.

Figure S3. Representative tSNE plots for 34 immune-related markers in patients with *EGFR*-mutated and wild-type surgically resected LUADs with CyTOF assays.

Figure S4. Graphical summary schema of two different mechanisms for Treg infiltration into the TME of *EGFR*-mutated and wild-type LUADs.

Figure S5. Relationships between clinical features (smoking status, tumor size and clinical stage) and $CD8^+$ T cell or Treg infiltration.

Figure S6. The comparable infiltration of TAMs, MDSCs and DCs in the TME of *EGFR*-mutated and wild-type LUADs with multi-fluorescent IHC.

Figure S7. GSEA of the differences in activated EGFR and inhibited EGFR signals in three NSCLC cell lines in microarray analyses.

Figure S8. *CCL5* expression in *EGFR*-mutated and wild-type NSCLC cell lines treated with erlotinib.

Figure S9. *CXCL10*, *CCL5* and *CCL22* expression and EGFR downstream signals in *EGFR*-mutated and wild-type NSCLC cell lines treated with a third-generation EGFR-tyrosine kinase inhibitor osimertinib.

Figure S10. EGFR expression by $CD8^+$ T cells and Tregs in PBMCs and their sensitivity to erlotinib.

Figure S11. *CXCL10* and *CCL22* expression in patients with *EGFR*-mutated LUADs before and after EGFR-tyrosine kinase inhibitor treatment.

Figure S12. The combination treatment with erlotinib and anti-PD-1 mAb effectively induces tumor growth inhibition with single clones of *EGFR* mutant (exon 19 deletion)-transfected MC-38.

Figure S13. *In vitro* proliferation and sensitivity to erlotinib in mock-transfected, wild-type and *EGFR* mutant (exon 19 deletion)-transfected MC-38 cell lines.

Figure S14. Changes in $CD8^+$ T cell and Treg infiltration in MC-39ex19del tumors following CXCL10 or CCL22 blockade administration, respectively.

Figure S15. Antitumor effects by the combination of erlotinib and anti-PD-1 mAb in MC-38ex19del tumors under Treg-depleted conditions induced by anti-CD25 mAb.

Figure S16. The changes in other chemokines induced by EGFR signaling in microarray analysis.

Table S1. Summary of LUADs patients who received surgery.

Table S2. Summary of LUAD patients who received EGFR-tyrosine kinase inhibitor therapy.

Table S3. Summary of antibodies used in the IHC.

Table S4. Summary of antibodies used in the CyTOF analyses.

Table S5. Summary of antibodies used in the flow cytometry analyses.

Table S6. Primers used in qRT-PCR.

Table S7. Summary of antibodies used in western blotting.

References and Notes:

1. T. S. Mok, Y. L. Wu, S. Thongprasert, C. H. Yang, D. T. Chu, N. Saijo, P. Sunpaweravong, B. Han, B. Margono, Y. Ichinose, Y. Nishiwaki, Y. Ohe, J. J. Yang, B. Chewaskulyong, H. Jiang, E. L. Duffield, C. L. Watkins, A. A. Armour, M. Fukuoka, Gefitinib or carboplatin-paclitaxel in pulmonary adenocarcinoma. *N Engl J Med* **361**, 947-957 (2009).

2. E. L. Kwak, Y. J. Bang, D. R. Camidge, A. T. Shaw, B. Solomon, R. G. Maki, S. H. Ou, B. J. Dezube, P. A. Janne, D. B. Costa, M. Varella-Garcia, W. H. Kim, T. J. Lynch, P. Fidias, H. Stubbs, J. A. Engelman, L. V. Sequist, W. Tan, L. Gandhi, M. Mino-Kenudson, G. C. Wei, S. M. Shreeve, M. J. Ratain, J. Settleman, J. G. Christensen, D. A. Haber, K. Wilner, R. Salgia, G. I. Shapiro, J. W. Clark, A. J. Iafrate, Anaplastic lymphoma kinase inhibition in non-small-cell lung cancer. *N Engl J Med* **363**, 1693-1703 (2010).

3. T. Mitsudomi, Y. Yatabe, Mutations of the epidermal growth factor receptor gene and related genes as determinants of epidermal growth factor receptor tyrosine kinase inhibitors sensitivity in lung cancer. *Cancer Sci* **98**, 1817-1824 (2007).

4. H. Borghaei, L. Paz-Ares, L. Horn, D. R. Spigel, M. Steins, N. E. Ready, L. Q. Chow, E. E. Vokes, E. Felip, E. Holgado, F. Barlesi, M. Kohlhäufl, O. Arrieta,

M. A. Burgio, J. Fayette, H. Lena, E. Poddubskaya, D. E. Gerber, S. N. Gettinger, C. M. Rudin, N. Rizvi, L. Crinò, G. R. Blumenschein, S. J. Antonia, C. Dorange, C. T. Harbison, F. Graf Finckenstein, J. R. Brahmer, Nivolumab versus Docetaxel in Advanced Nonsquamous Non-Small-Cell Lung Cancer. *N Engl J Med* **373**, 1627-1639 (2015).

5. M. Reck, D. Rodríguez-Abreu, A. G. Robinson, R. Hui, T. Csőszi, A. Fülöp, M. Gottfried, N. Peled, A. Tafreshi, S. Cuffe, M. O'Brien, S. Rao, K. Hotta, M. A. Leiby, G. M. Lubiniecki, Y. Shentu, R. Rangwala, J. R. Brahmer, K.-. Investigators, Pembrolizumab versus Chemotherapy for PD-L1-Positive Non-Small-Cell Lung Cancer. *N Engl J Med* **375**, 1823-1833 (2016).

6. W. Zou, J. D. Wolchok, L. Chen, PD-L1 (B7-H1) and PD-1 pathway blockade for cancer therapy: Mechanisms, response biomarkers, and combinations. *Sci Transl Med* **8**, 328rv324 (2016).

7. J. F. Gainor, A. T. Shaw, L. V. Sequist, X. Fu, C. G. Azzoli, Z. Piotrowska, T. G. Huynh, L. Zhao, L. Fulton, K. R. Schultz, E. Howe, A. F. Farago, R. J. Sullivan, J. R. Stone, S. Digumarthy, T. Moran, A. N. Hata, Y. Yagi, B. Y. Yeap, J. A. Engelman, M. Mino-Kenudson, EGFR Mutations and ALK Rearrangements Are Associated with Low Response Rates to PD-1 Pathway Blockade in Non-Small

Cell Lung Cancer: A Retrospective Analysis. *Clin Cancer Res* **22**, 4585-4593 (2016).

8. K. Ota, K. Azuma, A. Kawahara, S. Hattori, E. Iwama, J. Tanizaki, T. Harada, K. Matsumoto, K. Takayama, S. Takamori, M. Kage, T. Hoshino, Y. Nakanishi, I. Okamoto, Induction of PD-L1 Expression by the EML4-ALK Oncoprotein and Downstream Signaling Pathways in Non-Small Cell Lung Cancer. *Clin Cancer Res* **21**, 4014-4021 (2015).

9. N. Chen, W. Fang, J. Zhan, S. Hong, Y. Tang, S. Kang, Y. Zhang, X. He, T. Zhou, T. Qin, Y. Huang, X. Yi, L. Zhang, Upregulation of PD-L1 by EGFR Activation Mediates the Immune Escape in EGFR-Driven NSCLC: Implication for Optional Immune Targeted Therapy for NSCLC Patients with EGFR Mutation. *J Thorac Oncol* **10**, 910-923 (2015).

10. N. A. Rizvi, M. D. Hellmann, A. Snyder, P. Kvistborg, V. Makarov, J. J. Havel, W. Lee, J. Yuan, P. Wong, T. S. Ho, M. L. Miller, N. Rekhtman, A. L. Moreira, F. Ibrahim, C. Bruggeman, B. Gasmi, R. Zappasodi, Y. Maeda, C. Sander, E. B. Garon, T. Merghoub, J. D. Wolchok, T. N. Schumacher, T. A. Chan, Cancer immunology. Mutational landscape determines sensitivity to PD-1 blockade in non-small cell lung cancer. *Science* **348**, 124-128 (2015).

11. M. S. Rooney, S. A. Shukla, C. J. Wu, G. Getz, N. Hacohen, Molecular and genetic properties of tumors associated with local immune cytolytic activity. *Cell* **160**, 48-61 (2015).

12. M. Saito, Y. Shimada, K. Shiraishi, H. Sakamoto, K. Tsuta, H. Totsuka, S. Chiku, H. Ichikawa, M. Kato, S. Watanabe, T. Yoshida, J. Yokota, T. Kohno, Development of lung adenocarcinomas with exclusive dependence on oncogene fusions. *Cancer Res* **75**, 2264-2271 (2015).

13. S. L. Topalian, C. G. Drake, D. M. Pardoll, Immune checkpoint blockade: a common denominator approach to cancer therapy. *Cancer Cell* **27**, 450-461 (2015).

14. S. Spranger, R. M. Spaapen, Y. Zha, J. Williams, Y. Meng, T. T. Ha, T. F. Gajewski, Up-regulation of PD-L1, IDO, and Tregs in the melanoma tumor microenvironment is driven by $CD8^+$ T cells. *Sci Transl Med* **5**, 200ra116 (2013).

15. D. Q. Tran, H. Ramsey, E. M. Shevach, Induction of FOXP3 expression in naive human CD4+FOXP3 T cells by T-cell receptor stimulation is transforming growth factor-beta dependent but does not confer a regulatory phenotype. *Blood* **110**, 2983-2990 (2007).

16. M. Miyara, Y. Yoshioka, A. Kitoh, T. Shima, K. Wing, A. Niwa, C. Parizot, C. Taflin, T. Heike, D. Valeyre, A. Mathian, T. Nakahata, T. Yamaguchi, T. Nomura, M. Ono, Z. Amoura, G. Gorochov, S. Sakaguchi, Functional delineation and differentiation dynamics of human $CD4^+$ T cells expressing the FoxP3 transcription factor. *Immunity* **30**, 899-911 (2009).

17. T. Saito, H. Nishikawa, H. Wada, Y. Nagano, D. Sugiyama, K. Atarashi, Y. Maeda, M. Hamaguchi, N. Ohkura, E. Sato, H. Nagase, J. Nishimura, H. Yamamoto, S. Takiguchi, T. Tanoue, W. Suda, H. Morita, M. Hattori, K. Honda, M. Mori, Y. Doki, S. Sakaguchi, Two $FOXP3^+CD4^+$ T cell subpopulations distinctly control the prognosis of colorectal cancers. *Nat Med* **22**, 679-684 (2016).

18. Y. Togashi, H. Nishikawa, Regulatory T Cells: Molecular and Cellular Basis for Immunoregulation. *Curr Top Microbiol Immunol* **410**, 3-27 (2017).

19. K. Van Raemdonck, P. E. Van den Steen, S. Liekens, J. Van Damme, S. Struyf, CXCR3 ligands in disease and therapy. *Cytokine Growth Factor Rev* **26**, 311-327 (2015).

20. D. Peng, I. Kryczek, N. Nagarsheth, L. Zhao, S. Wei, W. Wang, Y. Sun, E. Zhao, L. Vatan, W. Szeliga, J. Kotarski, R. Tarkowski, Y. Dou, K. Cho, S. Hensley-

Alford, A. Munkarah, R. Liu, W. Zou, Epigenetic silencing of TH1-type chemokines shapes tumour immunity and immunotherapy. *Nature* **527**, 249-253 (2015).

21. O. Yoshie, K. Matsushima, CCR4 and its ligands: from bench to bedside. *Int Immunol* **27**, 11-20 (2015).

22. T. J. Curiel, G. Coukos, L. Zou, X. Alvarez, P. Cheng, P. Mottram, M. Evdemon-Hogan, J. R. Conejo-Garcia, L. Zhang, M. Burow, Y. Zhu, S. Wei, I. Kryczek, B. Daniel, A. Gordon, L. Myers, A. Lackner, M. L. Disis, K. L. Knutson, L. Chen, W. Zou, Specific recruitment of regulatory T cells in ovarian carcinoma fosters immune privilege and predicts reduced survival. *Nat Med* **10**, 942-949 (2004).

23. D. Liang, H. Xiao-Feng, D. Guan-Jun, H. Er-Ling, C. Sheng, W. Ting-Ting, H. Qin-Gang, N. Yan-Hong, H. Ya-Yi, Activated STING enhances Tregs infiltration in the HPV-related carcinogenesis of tongue squamous cells via the c-jun/CCL22 signal. *Biochim Biophys Acta* **1852**, 2494-2503 (2015).

24. P. C. Tseng, C. L. Chen, Y. S. Shan, C. F. Lin, An increase in galectin-3 causes cellular unresponsiveness to IFN-gamma-induced signal transduction and growth inhibition in gastric cancer cells. *Oncotarget* **7**, 15150-15160 (2016).

25. S. Matsuzaki, T. Ishizuka, T. Hisada, H. Aoki, M. Komachi, I. Ichimonji, M.

Utsugi, A. Ono, Y. Koga, K. Dobashi, H. Kurose, H. Tomura, M. Mori, F. Okajima, Lysophosphatidic acid inhibits CC chemokine ligand 5/RANTES production by blocking IRF-1-mediated gene transcription in human bronchial epithelial cells. *J Immunol* **185**, 4863-4872 (2010).

26. F. MacDonald, D. M. W. Zaiss, The Immune System's Contribution to the Clinical Efficacy of EGFR Antagonist Treatment. *Front Pharmacol* **8**, 575 (2017).

27. D. M. Zaiss, J. van Loosdregt, A. Gorlani, C. P. Bekker, A. Grone, M. Sibilia, P. M. van Bergen en Henegouwen, R. C. Roovers, P. J. Coffer, A. J. Sijts, Amphiregulin enhances regulatory T cell-suppressive function via the epidermal growth factor receptor. *Immunity* **38**, 275-284 (2013).

28. N. Nakamura, H. Chin, N. Miyasaka, O. Miura, An epidermal growth factor receptor/Jak2 tyrosine kinase domain chimera induces tyrosine phosphorylation of Stat5 and transduces a growth signal in hematopoietic cells. *J Biol Chem* **271**, 19483-19488 (1996).

29. A. Garcia-Diaz, D. S. Shin, B. H. Moreno, J. Saco, H. Escuin-Ordinas, G. A. Rodriguez, J. M. Zaretsky, L. Sun, W. Hugo, X. Wang, G. Parisi, C. P. Saus, D. Y. Torrejon, T. G. Graeber, B. Comin-Anduix, S. Hu-Lieskovan, R. Damoiseaux,

R. S. Lo, A. Ribas, Interferon Receptor Signaling Pathways Regulating PD-L1 and PD-L2 Expression. *Cell Rep* **19**, 1189-1201 (2017).

30. C. K. Lee, J. Man, S. Lord, M. Links, V. Gebski, T. Mok, J. C. Yang, Checkpoint Inhibitors in Metastatic EGFR-Mutated Non-Small Cell Lung Cancer-A Meta-Analysis. *J Thorac Oncol* **12***, 403-407* (2017).

31. M. A. Socinski, R. M. Jotte, F. Cappuzzo, F. Orlandi, D. Stroyakovskiy, N. Nogami, D. Rodríguez-Abreu, D. Moro-Sibilot, C. A. Thomas, F. Barlesi, G. Finley, C. Kelsch, A. Lee, S. Coleman, Y. Deng, Y. Shen, M. Kowanetz, A. Lopez-Chavez, A. Sandler, M. Reck, I. S. Group, Atezolizumab for First-Line Treatment of Metastatic Nonsquamous NSCLC. *N Engl J Med* **378**, 2288-2301 (2018).

32. T. Voron, E. Marcheteau, S. Pernot, O. Colussi, E. Tartour, J. Taieb, M. Terme, Control of the immune response by pro-angiogenic factors. *Front Oncol* **4**, 70 (2014).

33. F. Balkwill, Cancer and the chemokine network. *Nat Rev Cancer* **4**, 540-550 (2004).

34. E. Poole, C. A. King, J. H. Sinclair, A. Alcami, The UL144 gene product of human cytomegalovirus activates NFkappaB via a TRAF6-dependent

mechanism. *Embo j* **25**, 4390-4399 (2006).

35. N. Dixit, S. I. Simon, Chemokines, selectins and intracellular calcium flux: temporal and spatial cues for leukocyte arrest. *Front Immunol* **3**, 188 (2012).

36. M. D. Gunn, S. Kyuwa, C. Tam, T. Kakiuchi, A. Matsuzawa, L. T. Williams, H. Nakano, Mice lacking expression of secondary lymphoid organ chemokine have defects in lymphocyte homing and dendritic cell localization. *J Exp Med* **189**, 451-460 (1999).

37. Y. Takeuchi, A. Tanemura, Y. Tada, I. Katayama, A. Kumanogoh, H. Nishikawa, Clinical response to PD-1 blockade correlates with a sub-fraction of peripheral central memory CD4+ T cells in patients with malignant melanoma. *Int Immunol* **30**, 13-22 (2018).

38. K. Kataoka, Y. Nagata, A. Kitanaka, Y. Shiraishi, T. Shimamura, J. Yasunaga, Y. Totoki, K. Chiba, A. Sato-Otsubo, G. Nagae, R. Ishii, S. Muto, S. Kotani, Y. Watatani, J. Takeda, M. Sanada, H. Tanaka, H. Suzuki, Y. Sato, Y. Shiozawa, T. Yoshizato, K. Yoshida, H. Makishima, M. Iwanaga, G. Ma, K. Nosaka, M. Hishizawa, H. Itonaga, Y. Imaizumi, W. Munakata, H. Ogasawara, T. Sato, K. Sasai, K. Muramoto, M. Penova, T. Kawaguchi, H. Nakamura, N. Hama, K. Shide, Y. Kubuki, T. Hidaka, T. Kameda, T. Nakamaki, K. Ishiyama, S.

Miyawaki, S. S. Yoon, K. Tobinai, Y. Miyazaki, A. Takaori-Kondo, F. Matsuda, K. Takeuchi, O. Nureki, H. Aburatani, T. Watanabe, T. Shibata, M. Matsuoka, S. Miyano, K. Shimoda, S. Ogawa, Integrated molecular analysis of adult T cell leukemia/lymphoma. *Nat Genet* **47**, 1304-1315 (2015).

Acknowledgments:

We thank Dr. T. Morioka, Ms. T. Takaku, M. Nakai, K. Onagawa, M. Takemura, C. Haijima, M. Hoshino, K. Yoshida, C. Notake, H. Hashiguchi and J. Iemura for their technical assistance.

Funding:

This study was supported by Grants-in-Aid for Scientific Research [S grant no. 17H06162 (H.N.), Young Scientists no. 17J09900 (Y. Togashi), and JSPS Research fellow no. 17K18388 (Y. Togashi)] from the Ministry of Education, Culture, Sports, Science and Technology of Japan, and Technology of Japan, by the Project for Cancer Research, by Therapeutic Evolution (P-CREATE, no. 16cm0106301h0002, H.N.) from the Japan Agency for Medical Research and Development (AMED), by the National Cancer Center Research and Development Fund (no. 28-A-7 and 31-A-7, H.N.), by the Naito Foundation (Y. Togashi and H.N.), by the Takeda Foundation (Y. Togashi), by the SGH Foundation (Y. Togashi), by a Novartis Research Grant (Y. Togashi), and by the Kobayashi Foundation for Cancer Research (Y. Togashi). The analysis of immune status was executed in part as a research program supported by Ono Pharmaceutical Co., Ltd.

Author contributions:

E. Sugiyama. and Y. Togashi equally contributed to this work.

Y. Togashi and H.N. designed the research; E. Sugiyama, Y. Togashi, S.S., Y. Takeuchi, Y. Tada and K. Tane performed the experiments; K.G., Y.S., M.O. and M.T. obtained the clinical samples and data; E. Sugiyama, Y. Togashi, S.S., Y. Takeuchi, K.K., K.T., G.I., E. Sato. and H.N. analyzed the data; E. Sugiyama, Y. Togashi and H.N. wrote the paper.

Competing interests:

Y.T. has received honoraria and grants from Ono Pharmaceutical Co., Ltd., for this work, honoraria and grants from Bristol-Myers Squibb Co., Ltd., outside of this study, and honoraria from MSD. K.K., AstraZeneca. K.K., Boehringer Ingelheim GmbH, and Chugai Pharmaceutical Co., Ltd., outside this work. S.S. is an employee of Ono Pharmaceutical Co., Ltd. K.G. has received honoraria and grants from Ono Pharmaceutical Co., Ltd., MSD. K.K., Bristol-Myers Squibb Co., Ltd., Chugai Pharmaceutical Co., Ltd., Merck Serono, AstraZeneca. K.K., Boehringer Ingelheim GmbH and Pfizer Inc., outside of this study and honoraria from F. Hoffmann-La Roche Ltd. M.T. received honoraria from Ono Pharmaceutical Co., Ltd., outside of this study, honoraria and grants from Boehringer Ingelheim GmbH and MSD K.K. outside of this study, honoraria and grants from Chugai Pharmaceutical Co., Ltd., outside of study and

is a consultant of MSD K.K. and Chugai Pharmaceutical Co., Ltd., outside of the study. H.N. received honoraria and grants from Ono Pharmaceutical Co., Ltd., for this work, honoraria and grants from Bristol-Myers Squibb Co., Ltd. and Chugai Pharmaceutical Co., Ltd., and grants from Taiho Pharmaceutical, Daiichi-Sankyo, Kyowa Kirin, Merck Serono, Zenyaku Kogyo, Astellas Pharmaceutical, Asahi Kasei, Sysmex, and BD Japan outside of this study. Other authors declare no competing financial interests.

Data availability statement:

The data discussed in this publication is under submission in NCBIs Gene Expression Omnibus (GEO, http://www.ncbi.nlm.nih.gov/geo/).

Figures:

Fig. 1. Immune-related gene expression and tumor mutation burden are decreased in *EGFR*-mutated LUADs.

A. Heatmap of RNAseq from surgically resected LUADs. Nineteen LUAD samples were subjected to RNAseq and clustered by previously reported gene sets ($CD4^+$ Tregs, $CD8^+$ T cells, macrophages, dendritic cells, MHC class I, costimulatory APCs and T cells, coinhibitory APCs and T cells, IFN response, and cytolytic activity) (*11*). MT, *EGFR*-mutated; BI, Brinkman index. **B.** Gene expression of *CD274, CD8A* and *PRF1* according to *EGFR* gene status. **C.** Representative IHC for PD-L1, CD8 and FOXP3 according to *EGFR* gene status (Top). Summary of PD-L1 expression and the ratio of FOXP3/CD8 (bottom). **D.** Tumor mutation burden according to *EGFR* gene status. Both single nucleotide variants and SNP and frameshift mutations were examined.

Fig. 2. Tregs highly infiltrate into *EGFR*-mutated LUADs with a non-inflamed TME.

A. TILs from *EGFR*-mutated and wild-type LUADs were subjected to CyTOF assays, and representative tSNE plots (CD4, CD8, FOXP3 and PD-1) are shown. **B.** (Left) Representative flow cytometry staining (CD4/CD8 for T cells and CD45RA/FOXP3 for $CD4^+$ T cells) of TILs from *EGFR*-mutated and wild-type LUADs. (Right) Summary of the frequency of the indicated T cell fractions in surgically resected LUADs. Fr. I, fraction I (naive Tregs); Fr. II, fraction II (effector Tregs); Fr. III, fraction III (non-Tregs); *EGFR* MT, *EGFR* mutations.

Fig. 3. CXCL10 recruiting $CD8^+$ effector T cells is down-regulated and CCL22 recruiting Tregs is up-regulated by EGFR signal in *EGFR*-mutated LUADs.

A. Two *EGFR*-mutated cell lines (PC-9 and HCC827) and an *EGFR* wild-type cell line (H322) treated with erlotinib and EGF, respectively, were subjected to microarray analysis. GO terms, cytokines and chemokines were examined. **B.** *CXCL10* and *CCL22* expression levels in the *EGFR*-mutated cell lines (PC-9 and HCC827) treated with/without erlotinib and the *EGFR* wild-type cell line (H322) treated with/without EGF and erlotinib was evaluated by quantitative real-time reverse transcription PCR. **C.** The concentrations of CXCL10 and CCL22 in the cultured medium of the *EGFR*-mutated cell lines (PC-9 and HCC827) treated with/without erlotinib and the *EGFR* wild-type cell line (H322) treated with/without EGF and erlotinib were examined by ELISAs. Data are shown from three independent experiments.

Fig. 4. EGFR signaling controls the transcription factors *cJun/JNK* and *IRF1* for the immune phenotype of *EGFR*-mutated LUADs.

A. Two *EGFR*-mutated cell lines (PC-9 and HCC827) and an *EGFR* wild-type cell line (H322) treated with erlotinib and EGF, respectively, were subjected to microarray analysis. The expression of transcription factors was examined. **B.** *JUN* and *IRF1* expression in the *EGFR*-mutated cell lines (PC-9 and HCC827) with/without erlotinib and the *EGFR* wild-type cell line (H322) treated with/without EGF and erlotinib were evaluated by quantitative real-time reverse transcription PCR. **C.** PC-9 (*EGFR*-mutated cell line) treated with/without erlotinib and H322 (*EGFR* wild-type cell line) were treated with/without EGF and erlotinib, and transcription factor expression was examined with western blotting. **D.** (Left) *JUN* expression by PC-9 was knocked down by siRNA, and protein expression was confirmed with western blotting. (Right) *CXCL10* and *CCL22* gene expression was examined by quantitative real-time reverse transcription PCR, and luciferase activity of the *CXCL10* and *CCL22* promoter regions was examined by luciferase assays. **E.** *IRF1* expression by PC-9 was knocked down by siRNA, and protein expression was confirmed with western blotting. (Right) *CXCL10* and *CCL22* gene expression was examined by quantitative real-time reverse transcription PCR, and luciferase activity of the *CXCL10* and *CCL22* promoter regions was examined by

luciferase assays. Data from three independent experiments are shown.

Fig. 5. The combination treatment with erlotinib and anti-PD-1 mAb effectively induces tumor growth inhibition in *EGFR*-mutated LUADs.

A. (Left) Representative flow cytometry staining (CD45RA/FOXP3 for $CD4^+$ T cells) of TILs and (Right) a summary of advanced LUAD patients treated with EGFR-tyrosine kinase inhibitors. TILs were collected pre- and post-EGFR-tyrosine kinase inhibitor treatment and subjected to flow cytometry. **B.** Human *EGFR* wild-type or mutant (exon 19 deletion)-transfected MC-38 mouse cell line (MC-38wt or MC-38Ex19del, respectively) was established, and human EGFR expression, phospho-EGFR, and exon 19-deleted EGFR were confirmed by western blotting. **C.** Mice were inoculated with MC-38wt or MC-38Ex19del with/without erlotinib treatment, and tumor-infiltrating Tregs and $CD8^+$ T cells were analyzed. (Left) Representative flow cytometry staining of TILs and (Right) a summary of the frequency of Tregs, $CD8^+$ T cells and ratio of FOXP3/CD8. **D.** CXCL10, CCL22, CCL5, IRF1 and JUN expression levels in MC-38wt and MC-38ex19del with/without erlotinib were evaluated by qRT-PCR. Mice were inoculated with MC-38wt or MC-38ex19del with/without erlotinib treatment. Tumors were collected on day 8, and CXCL10, CCL22, CCL5, IRF1 and JUN expression was analyzed with qRT-PCR. **E.** Mice were inoculated with MC-38mock or MC-38wt or MC-38Ex19del and treated with/without erlotinib, anti-PD-1 mAb or the combination (erlotinib + anti-PD-1

mAb). Tumor growth and the survival curve are shown. Representative data from two independent experiments are shown. n.s., not significant. **F.** Human *EGFR* wild-type or mutant (exon 19 deletion)-transfected LL/2 mouse cell line (LL/2wt or LL/2ex19del, respectively) was established, and human EGFR expression, phospho-EGFR, and exon 19-deleted EGFR were confirmed by western blotting. **G**. Mice were intravenously administered with LL/2ex19del and treated with/without erlotinib, anti-PD-1 mAb or a combination (erlotinib + anti-PD-1 mAb). A summary of lung weights with tumors is shown. Representative data are shown from two independent experiments.

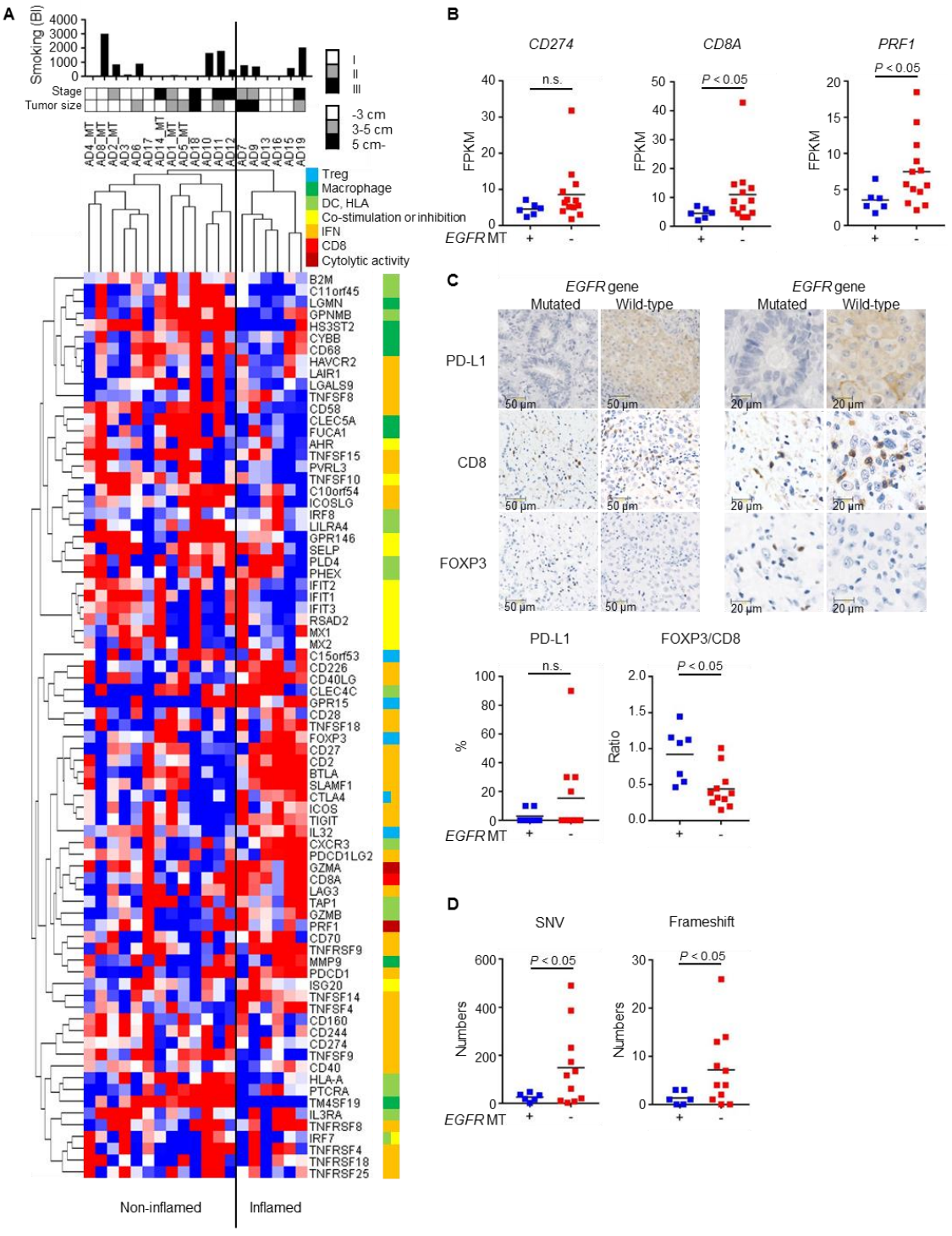
A
Smoking (BI)
Stage
Tumor size
I
II
III
-3 cm
3-5 cm
5 cm-
Treg
Macrophage
DC, HLA
Co-stimulation or inhibition
IFN
CD8
Cytolytic activity
Non-inflamed
Inflamed
B
CD274
CD8A
PRF1
n.s.
P < 0.05
FPKM
EGFR MT
C
EGFR gene
Mutated
Wild-type
PD-L1
CD8
FOXP3
50 μm
20 μm
FOXP3/CD8
%
Ratio
D
SNV
Frameshift
Numbers

Figure 1

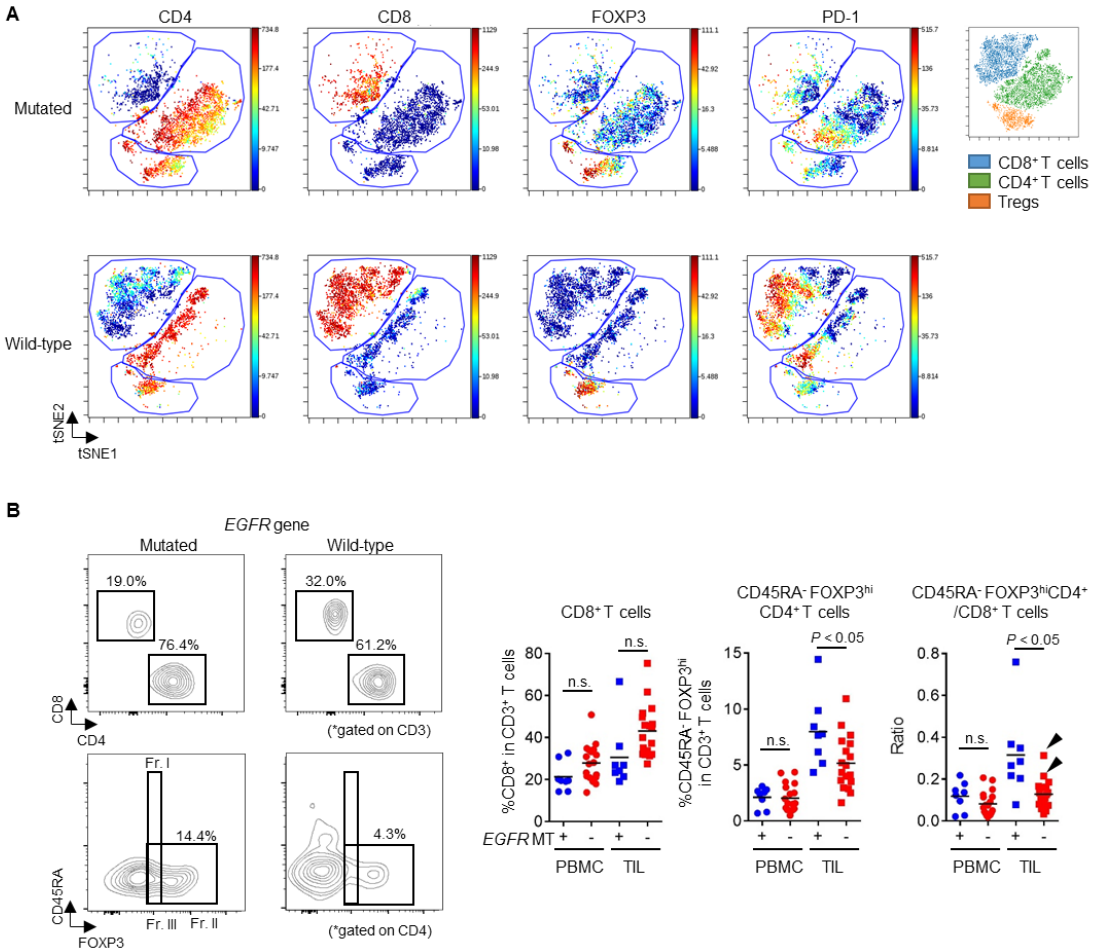
A
CD4
CD8
FOXP3
PD-1
Mutated
Wild-type
CD8+ T cells
CD4+ T cells
Tregs
tSNE2
tSNE1
B
EGFR gene
Mutated
Wild-type
19.0%
76.4%
32.0%
61.2%
CD8
CD4
(*gated on CD3)
Fr. I
14.4%
4.3%
CD45RA
FOXP3
Fr. III
Fr. II
(*gated on CD4)
CD8+ T cells
%CD8+ in CD3+ T cells
n.s.
EGFR MT + - + -
PBMC
TIL
CD45RA- FOXP3hi CD4+ T cells
%CD45RA- FOXP3hi in CD3+ T cells
P < 0.05
CD45RA- FOXP3hi CD4+ /CD8+ T cells
Ratio

Figure 2

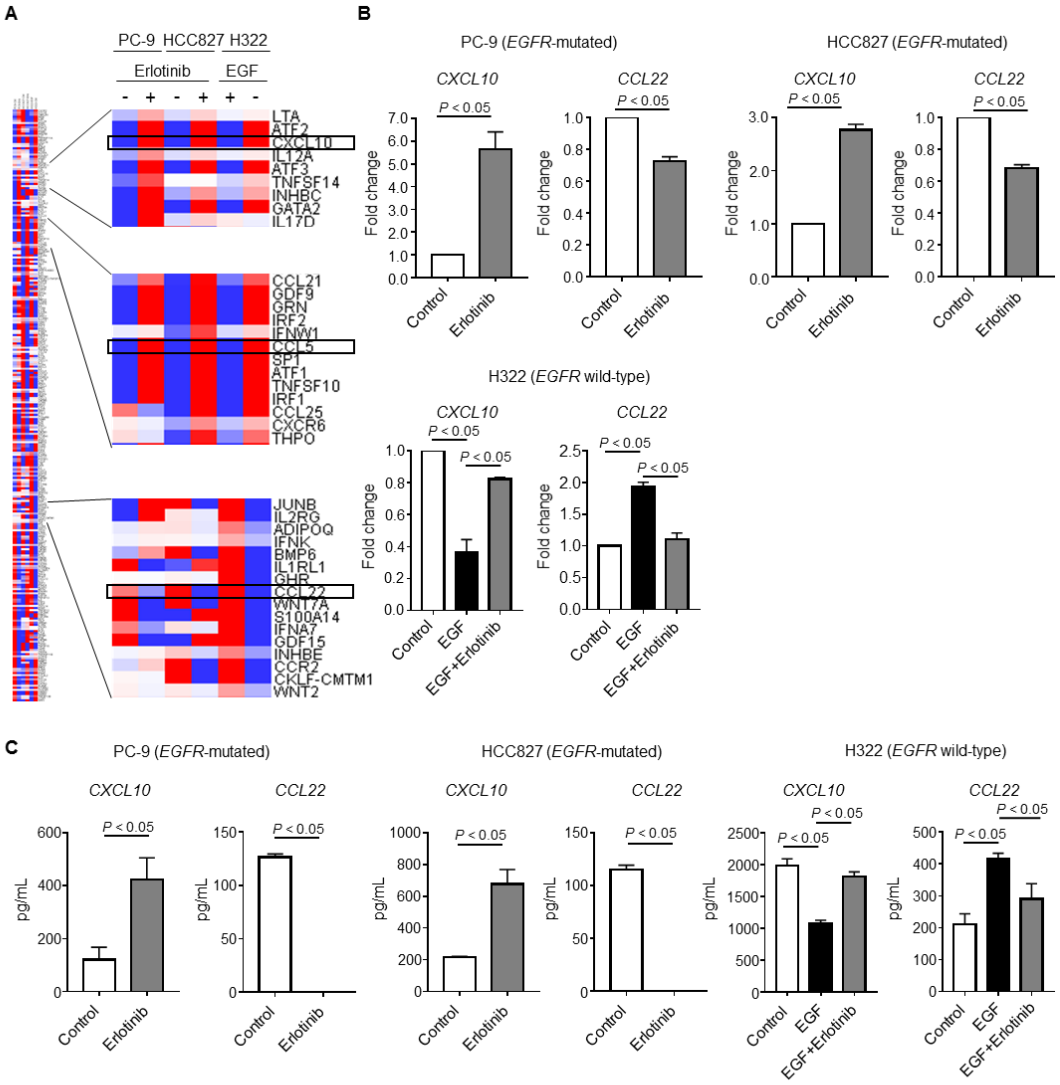
A
PC-9 HCC827 H322
Erlotinib EGF
- + - + + -
LTA
ATF2
CXCL10
IL12A
ATF3
TNFSF14
INHBC
GATA2
IL17D
CCL21
GDF9
GRN
IRF2
IFNW1
CCL5
SP1
ATF1
TNFSF10
IRF1
CCL25
CXCR6
THPO
JUNB
IL2RG
ADIPOQ
IFNK
BMP6
IL1RL1
GHR
CCL22
WNT7A
S100A14
IFNA7
GDF15
INHBE
CCR2
CKLF-CMTM1
WNT2
B
PC-9 (EGFR-mutated)
CXCL10
CCL22
P < 0.05
Fold change
Control
Erlotinib
HCC827 (EGFR-mutated)
H322 (EGFR wild-type)
Control
EGF
EGF+Erlotinib
C
pg/mL

Figure 3

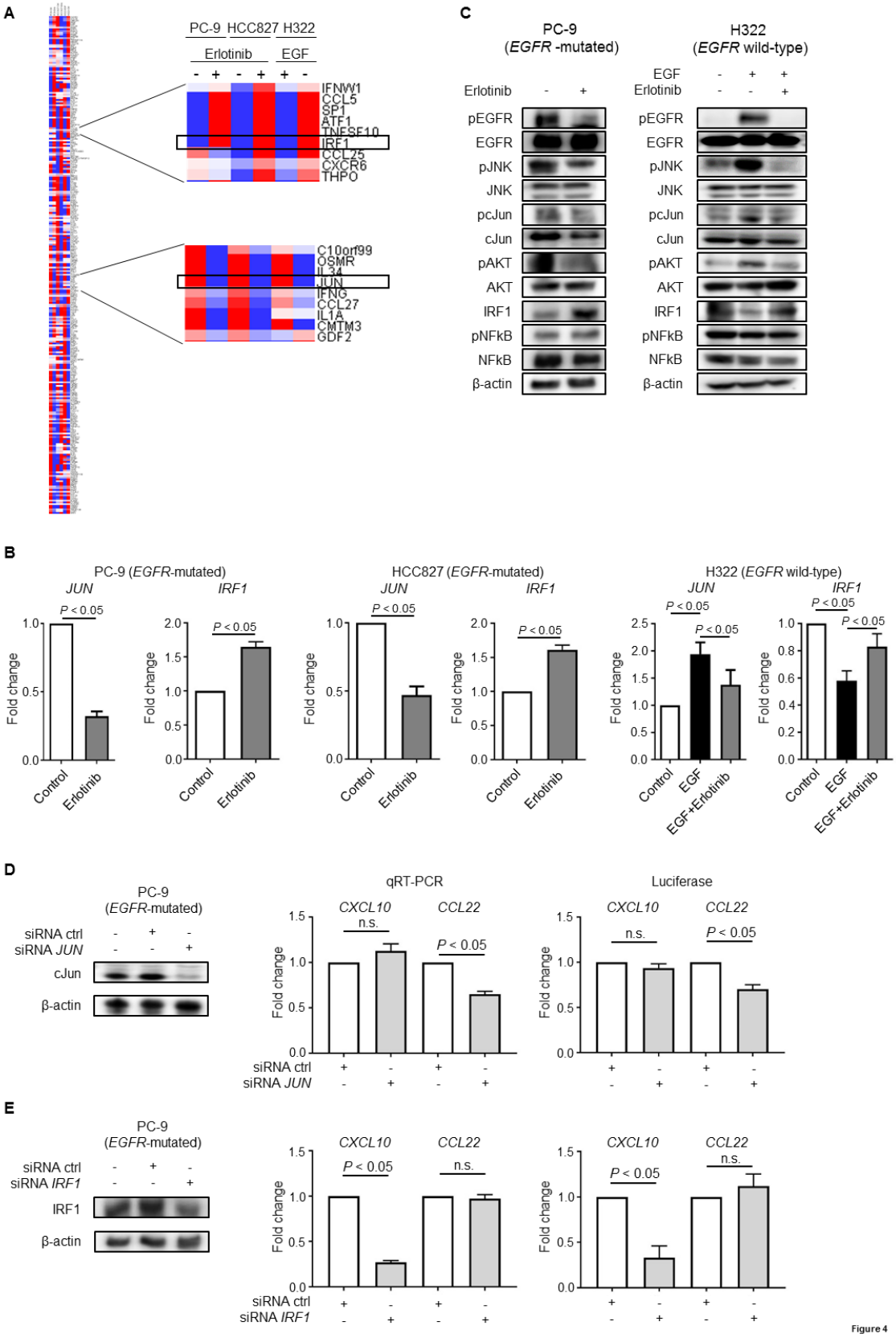
A
PC-9 HCC827 H322
Erlotinib
EGF
IFNW1
CCL5
SP1
ATF1
TNFSF10
IRF1
CCL25
CXCR6
THPO
C10orf99
OSMR
IL34
JUN
IFNG
CCL27
IL1A
CMTM3
GDF2
C
PC-9
(EGFR -mutated)
H322
(EGFR wild-type)
Erlotinib
EGF
pEGFR
EGFR
pJNK
JNK
pcJun
cJun
pAKT
AKT
IRF1
pNFkB
NFkB
β-actin
B
PC-9 (EGFR-mutated)
HCC827 (EGFR-mutated)
H322 (EGFR wild-type)
JUN
IRF1
P < 0.05
Fold change
Control
Erlotinib
EGF
EGF+Erlotinib
D
PC-9
(EGFR-mutated)
siRNA ctrl
siRNA JUN
cJun
β-actin
qRT-PCR
Luciferase
CXCL10
CCL22
n.s.
E
siRNA IRF1
IRF1

Figure 4

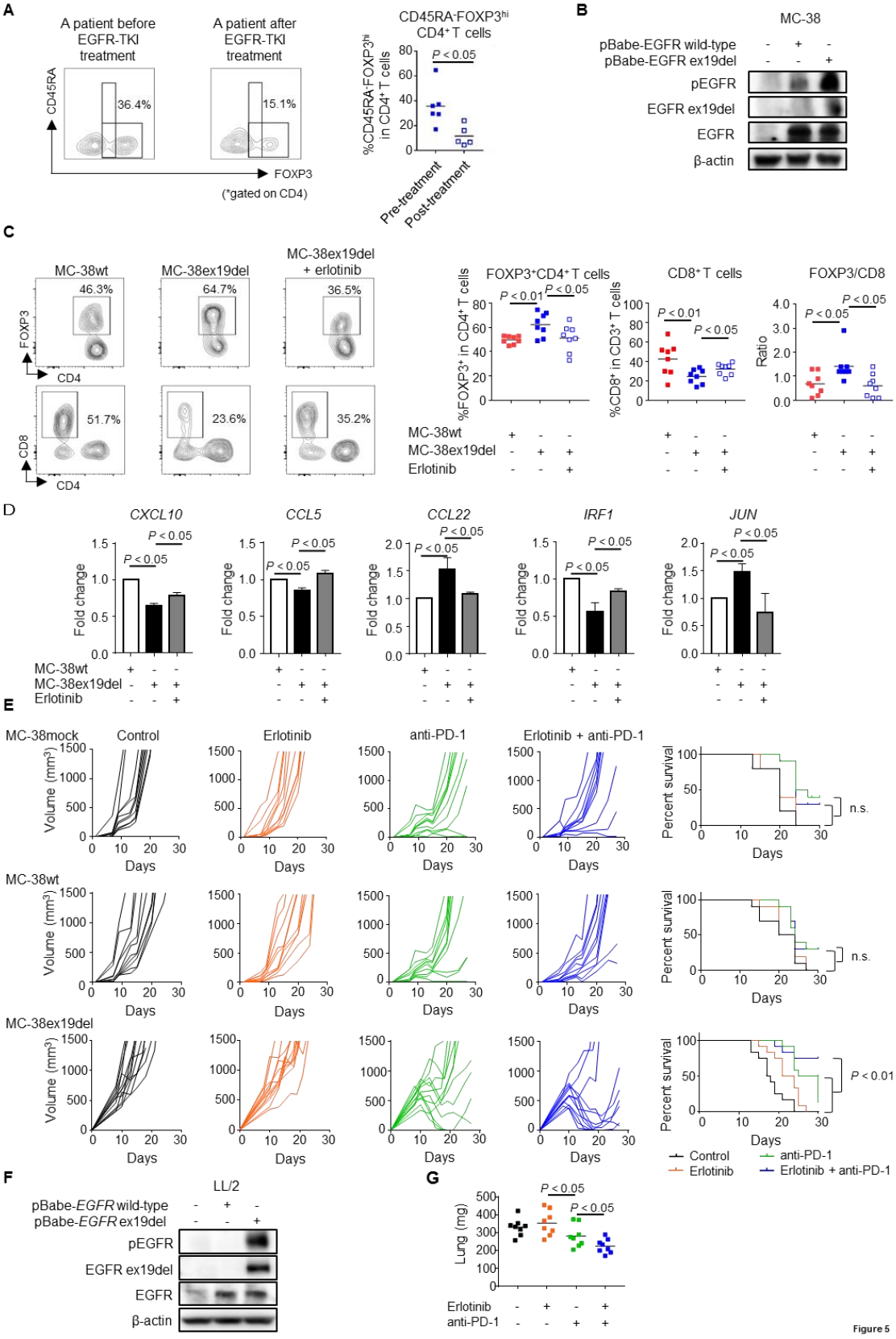
A
A patient before EGFR-TKI treatment
A patient after EGFR-TKI treatment
CD45RA
36.4%
15.1%
FOXP3
(*gated on CD4)
CD45RA-FOXP3hi CD4+ T cells
%CD45RA-FOXP3hi in CD4+ T cells
P < 0.05
Pre-treatment
Post-treatment
B
MC-38
pBabe-EGFR wild-type
pBabe-EGFR ex19del
pEGFR
EGFR ex19del
EGFR
β-actin
C
MC-38wt
MC-38ex19del
MC-38ex19del + erlotinib
46.3%
64.7%
36.5%
FOXP3
CD4
51.7%
23.6%
35.2%
CD8
FOXP3+CD4+ T cells
%FOXP3+ in CD4+ T cells
CD8+ T cells
%CD8+ in CD3+ T cells
FOXP3/CD8
Ratio
P < 0.01
P < 0.05
MC-38wt
MC-38ex19del
Erlotinib
D
CXCL10
CCL5
CCL22
IRF1
JUN
Fold change
E
MC-38mock
MC-38wt
MC-38ex19del
Control
Erlotinib
anti-PD-1
Erlotinib + anti-PD-1
Volume (mm3)
Days
Percent survival
n.s.
P < 0.01
F
LL/2
pBabe-EGFR wild-type
pBabe-EGFR ex19del
pEGFR
EGFR ex19del
EGFR
β-actin
G
Lung (mg)
Erlotinib
anti-PD-1

Figure 5

Supplementary Materials:

Fig. S1. Comparable *CD274* expression between *EGFR*-mutated and *EGFR* wild-type NSCLC cell lines after IFN-γ treatment.

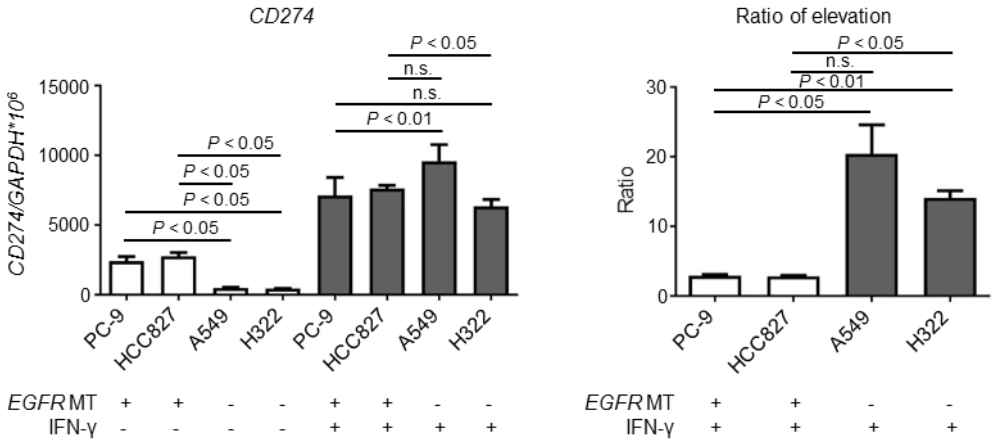

(Left) *CD274* expression with/without IFN-γ treatment in *EGFR*-mutated (PC-9 and HCC827) and *EGFR* wild-type (A549 and H322) NSCLC cell lines was examined by qRT-PCR. (Right) Elevated ratio of *CD274* expression before and after IFN-γ treatment. Data from three independent experiments are shown. n.s., not significant.

Fig. S2. The expression of *CD274* and other immune-related genes and tumor mutation burden in *EGFR*-mutated and wild-type LUADs in our cohort and TCGA data.

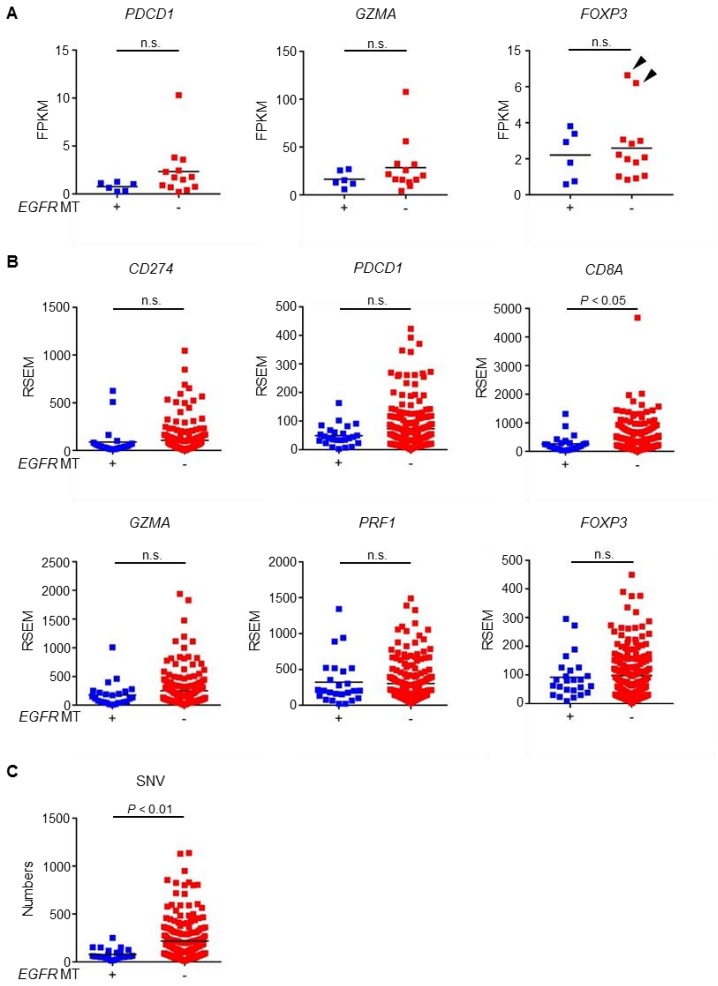

A. The expression of immune-related genes (*PDCD1*, *GZMA* and *FOXP3*) was examined with RNAseq according to *EGFR* gene status. **B.** The expression of immune-related genes (*CD274*, *PDCD1*, *CD8A*, *GZMA*, *PRF1* and *FOXP3*) was validated with the TCGA data**. C.** TMB according to the *EGFR* gene status in the TCGA data. SNP,

single nucleotide variants. n.s., not significant.

Fig. S3. Representative tSNE plots for 34 immune-related markers in patients with *EGFR*-mutated and wild-type surgically resected LUADs with CyTOF assays.

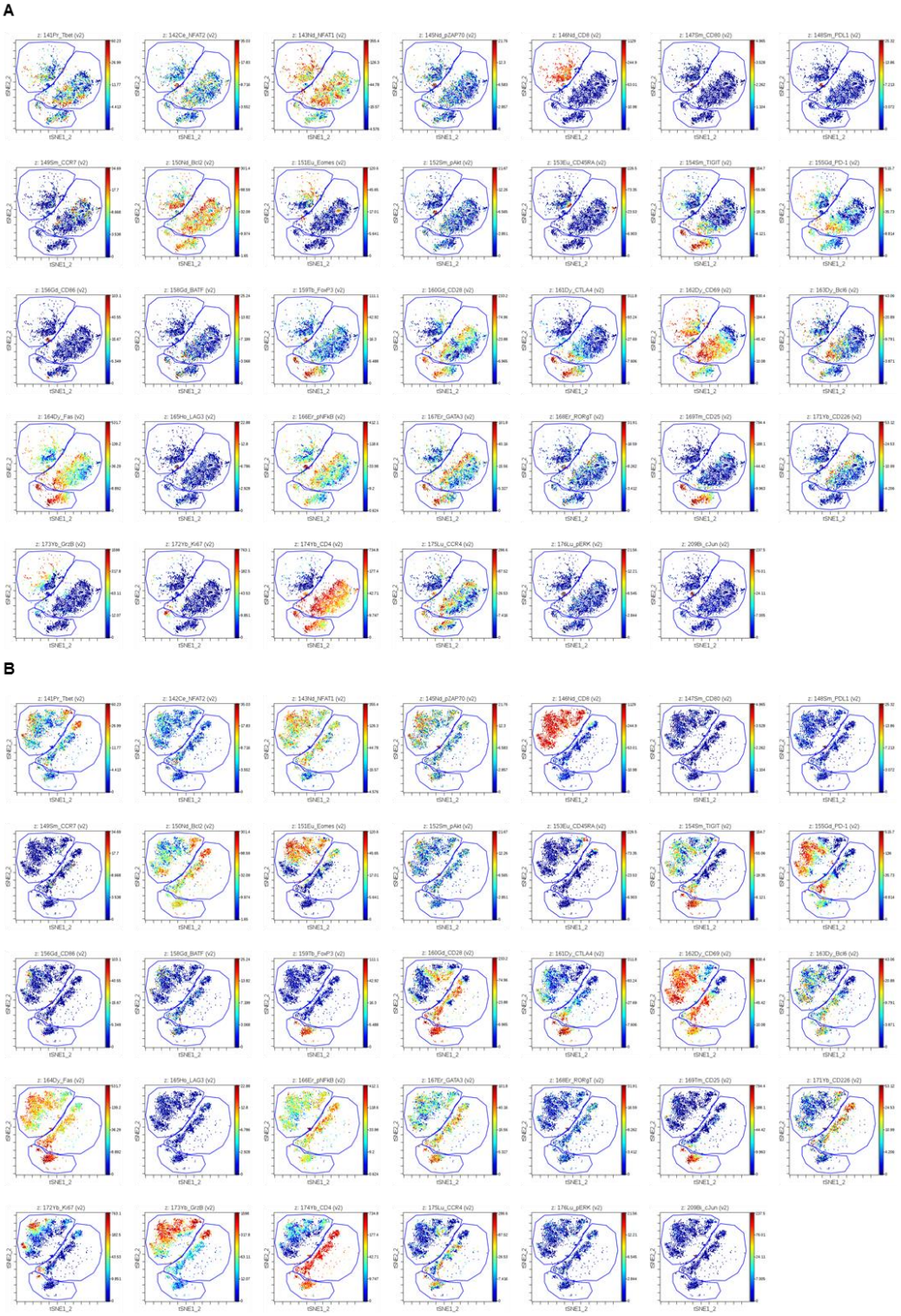

TILs from *EGFR*-mutated (**A**) and wild-type (**B**) LUADs were subjected to CyTOF assays, and representative tSNE plots (34 markers) are shown.

Fig. S4. Graphical summary schema of two different mechanisms for Treg infiltration into the TME of *EGFR*-mutated and wild-type LUADs.

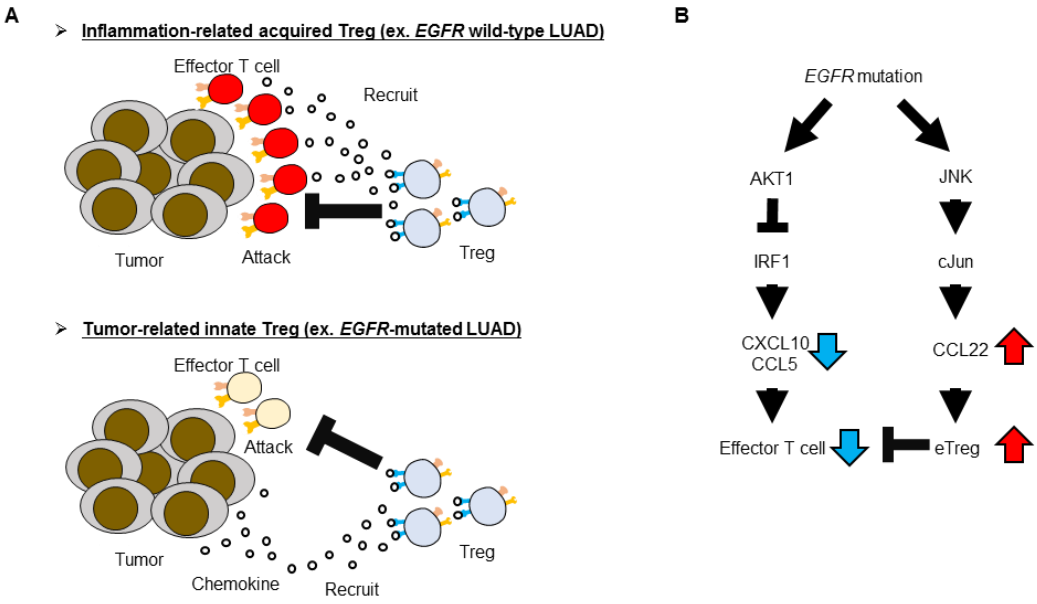

A. A concept of Treg infiltration into the TME: "Inflammation-related acquired Tregs" (top) and "Tumor-related innate Tregs" (bottom). In "Inflammation-related acquired Tregs", T cells and/or immune cells such as macrophages infiltrate into the tumor tissues and develop a dysfunctional state. These dysfunctional immune cells, particularly T cells, produce chemokines to recruit Tregs. In "Tumor-related innate Tregs", tumor cells themselves produce chemokines such as CCL22 to recruit Tregs as a mechanism of immune escape, as described in the cancer immunoediting hypothesis.

B. The mechanism of Treg infiltration in *EGFR*-mutated LUAD. EGFR signaling activated the MAPK pathway (*cJun/JNK*) and reduced *IRF1*; the former increased *CCL22* recruitment of eTregs, and the latter decreased *CXCL10* and *CCL5* induction of $CD8^+$ T-

cell infiltration, resulting in a immunological status in the TME: high Treg infiltration despite low $CD8^+$ effector T cell infiltration.

Fig. S5. Relationships between clinical features (smoking status, tumor size and clinical stage) and CD8$^+$ T cell or Treg infiltration.

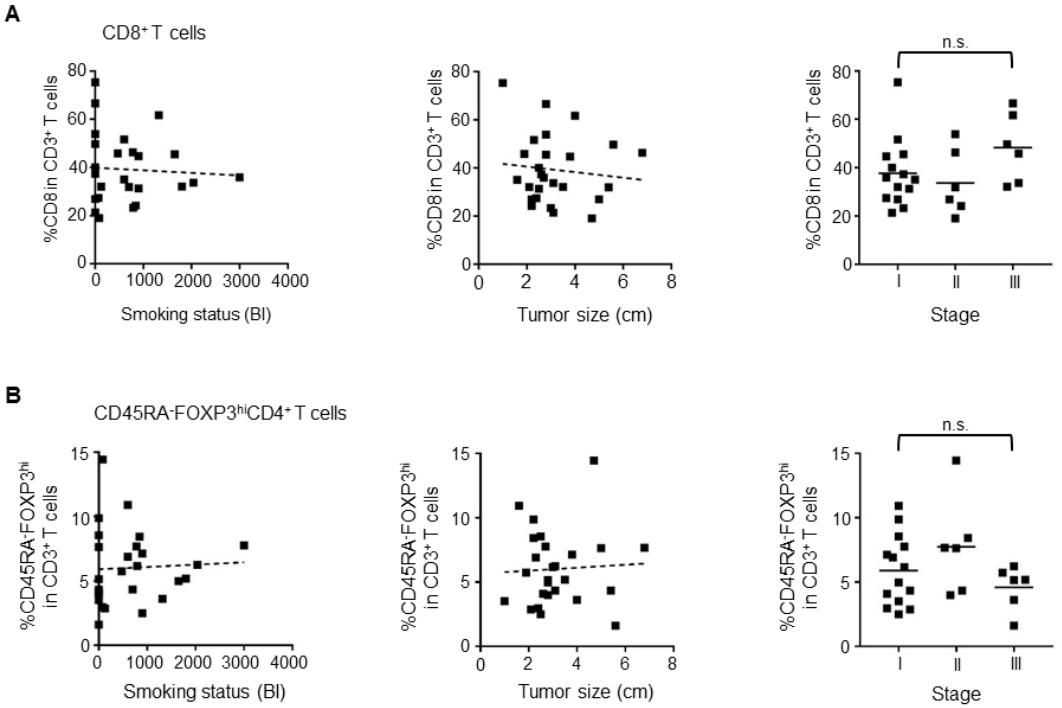

Relationships between CD8$^+$ T cell (**A**) or eTreg (**B**) infiltration and smoking status, tumor size, or pathological stage are analyzed. BI, Brinkman index; n.s., not significant.

Fig. S6. The comparable infiltration of TAMs, MDSCs and DCs in the TME of *EGFR*-mutated and wild-type LUADs with multi-fluorescent IHC.

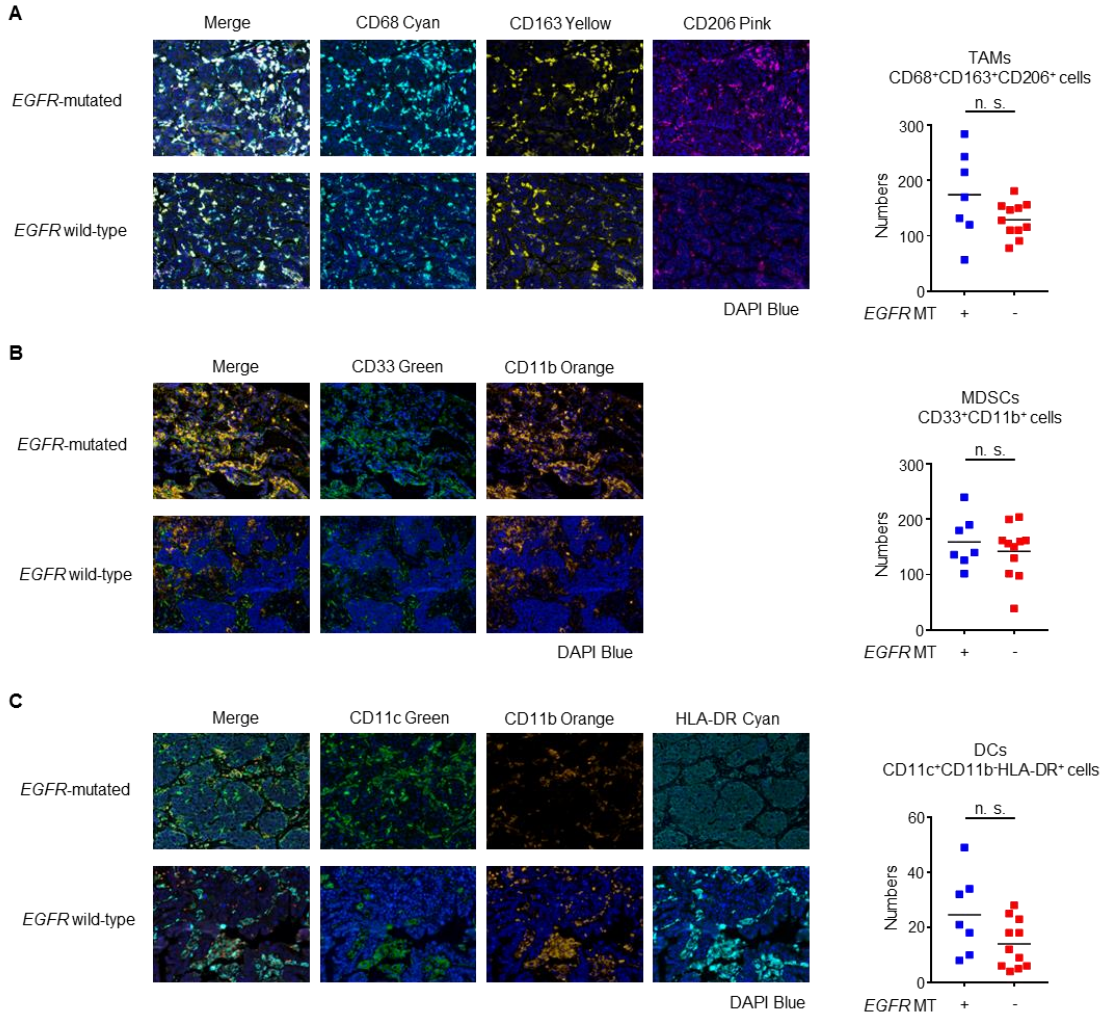

Representative multi-fluorescence findings (left) for (**A**) TAMs ($CD68^+CD163^+CD206^+$ cells), (**B**) MDSCs ($CD33^+CD11b^+$ cells) and (**C**) DCs ($CD11c^+CD11b^-HLA\text{-}DR^+$ cells) and summaries (right) according to *EGFR* gene status. n.s., not significant.

Fig. S7. GSEA of the differences in activated and inhibited EGFR signals in three NSCLC cell lines in microarray analyses.

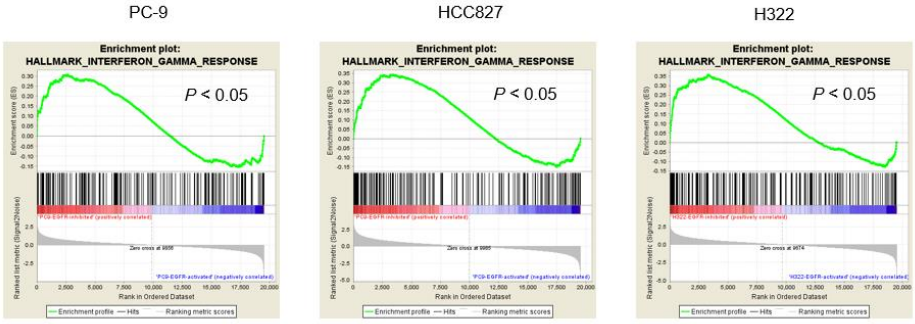

GSEA was carried out to analyze the differences between two groups: activated EGFR signals and inhibited EGFR signals in 3 NSCLC cell lines (PC-9, HCC827 and H322). The gene sets were adopted from The Molecular Signatures Database. The phenotype label was EGFR activation score vs. EGFR inhibition score.

Fig. S8. *CCL5* expression in *EGFR*-mutated and wild-type NSCLC cell lines treated with erlotinib.

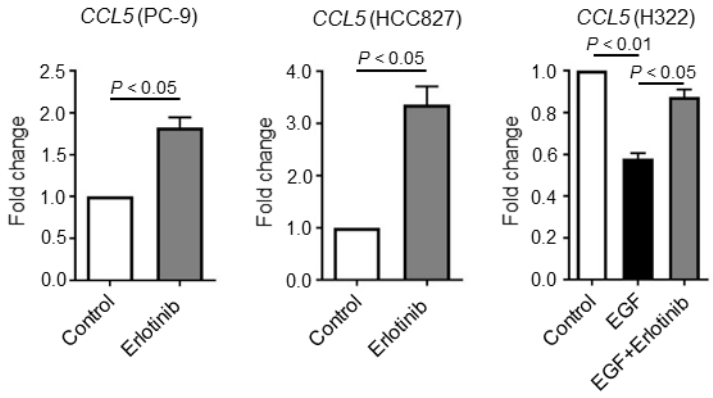

CCL5 expression in *EGFR*-mutated cell lines (PC-9 and HCC827) treated with/without erlotinib and an *EGFR* wild-type cell line (H322) treated with/without EGF and erlotinib were evaluated by qRT-PCR. Data from three independent experiments are shown.

Fig S9. *CXCL10*, *CCL5* and *CCL22* expression and EGFR downstream signals in *EGFR*-mutated and wild-type NSCLC cell lines treated with a third-generation EGFR-tyrosine kinase inhibitor osimertinib.

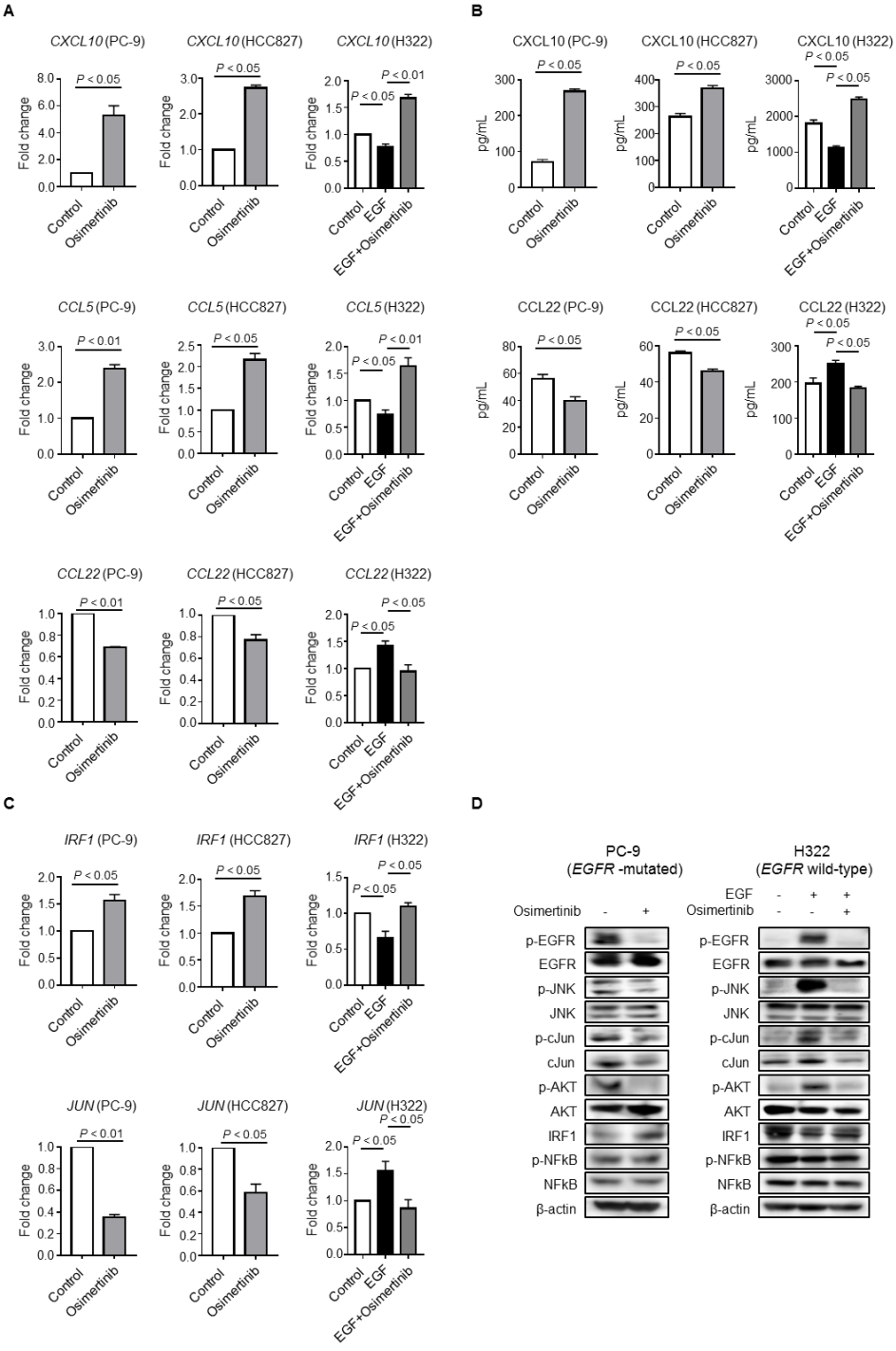

The expression levels of *CXCL10, CCL22* and *CCL5* in *EGFR*-mutated cell lines (PC-9 and HCC827) treated with/without the third-generation EGFR-tyrosine kinase inhibitor osimertinib and an *EGFR* wild-type cell line (H322) treated with/without EGF and osimertinib were evaluated with qRT-PCR **(A)** and ELISAs **(B)**. The expression levels of *IRF1* and *JUN* in *EGFR*-mutated cell lines (PC-9 and HCC827) treated with/without osimertinib and an *EGFR* wild-type cell line (H322) treated with/without EGF and osimertinib were examined with qRT-PCR (**C**). EGFR downstream signals were analyzed with western blotting **(D)**. Data from three independent experiments are shown.

Fig. S10. EGFR expression by CD8⁺ T cells and Tregs in PBMCs and their sensitivity to erlotinib.

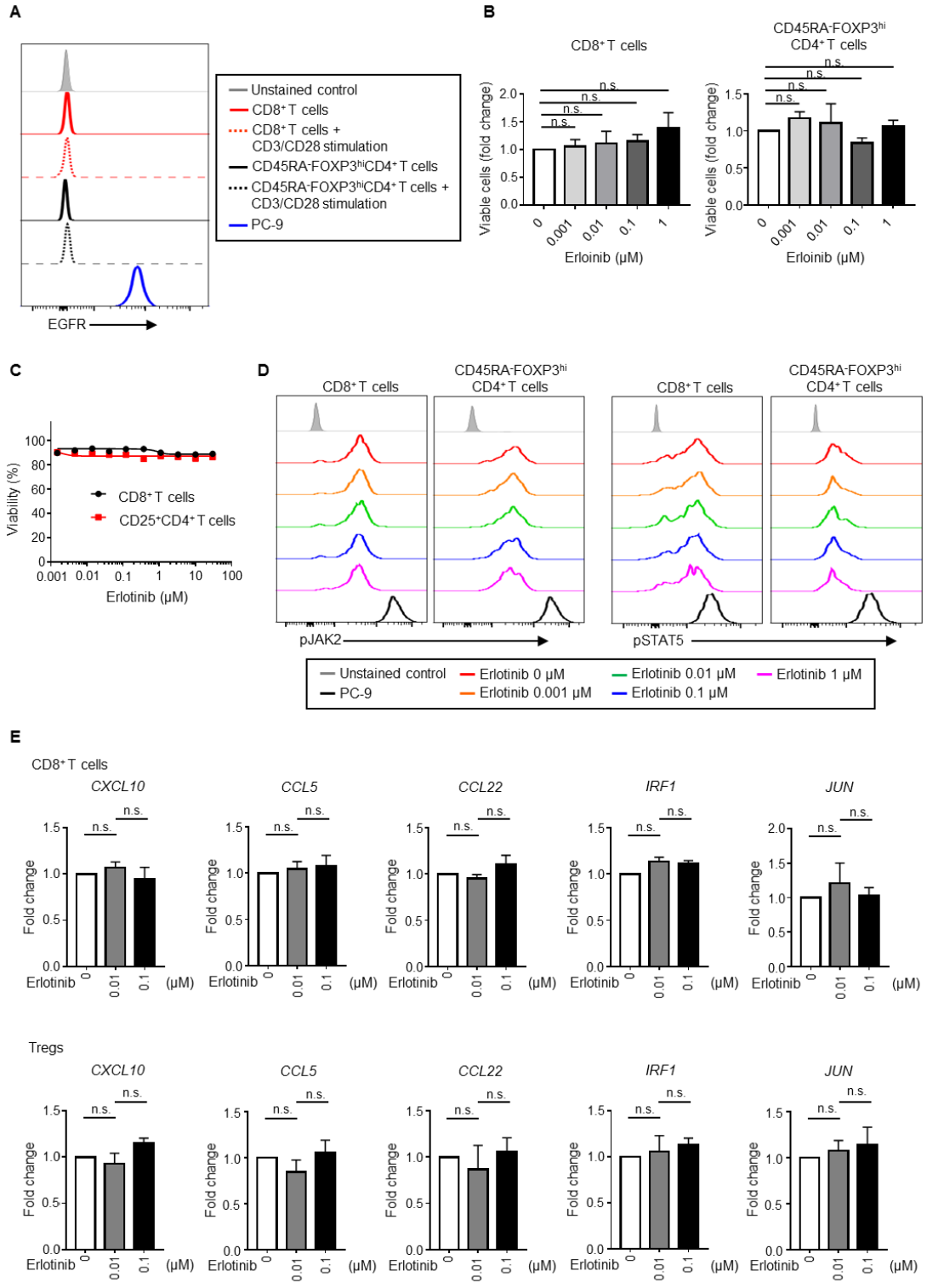

A. EGFR expression by $CD8^+$ T cells and $FOXP3^{high}CD45RA^-CD4^+$ T cells. EGFR expression was analyzed by flow cytometry using PBMCs from healthy individuals treated with/without CD3/CD28 Dynabeads and the PC-9 cell line (an *EGFR*-mutated NSCLC cell line). Representative flow cytometry staining is shown. **B.** Viabilities of human $CD8^+$ T cells and $FOXP3^{high}CD45RA^-CD4^+$ T cells. PBMCs were cultured with erlotinib (0, 0.001, 0.01, 0.1, and 1 μM) for 48 hours, and viable cell numbers were quantified with flow cytometry. **C.** Sensitivity to erlotinib in mouse $CD8^+$ T cells and Tregs ($CD25^+CD4^+$ T cells). After $CD8^+$ T cells and Tregs sorted from the spleen of C57BL/6 mice were cultured at a density of 1×10^4 cells/well in a 96-well plate with erlotinib for 48 hours, sensitivity was analyzed by WST-1 assays. **D.** pJAK2 and pSTAT5 expression in $CD8^+$ T cells and $FOXP3^{high}CD45RA^-CD4^+$ T cells treated with CD3/CD28 Dynabeads. Phospho-JAK2 and phospho-STAT5 expression were analyzed by flow cytometry using PBMCs treated with erlotinib for 48 hours. **E.** *CXCL10*, *CCL22*, *CCL5*, *IRF1* and *JUN* expression in $CD8^+$ T cells (top) and Tregs ($CD25^+CD4^+$ T cells) (bottom). $CD8^+$ T cells and Tregs sorted from the spleen of C57BL/6 mice were treated with/without erlotinib for 6 hours, and *CXCL10*, *CCL22*, *CCL5*, *IRF1* and *JUN* expression levels were analyzed by qRT-PCR. Data from three independent experiments are shown. n.s., not significant.

Fig. S11. *CXCL10* and *CCL22* expression in patients with *EGFR*-mutated LUADs before and after EGFR- tyrosine kinase inhibitor treatment.

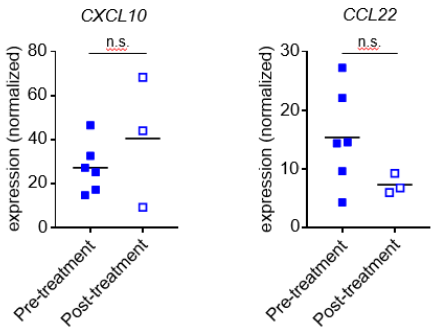

RNA was extracted from FFPE specimens of *EGFR*-mutated LUADs before and after EGFR-tyrosine kinase inhibitor treatment and was subjected to *CXCL10* and *CCL22* expression analyses using the nCounter platform. Data were normalized with nSolver analysis software. n.s., not significant.

Fig. S12. The combination treatment with erlotinib and anti-PD-1 mAb effectively induces tumor growth inhibition with single clones of *EGFR* mutant (exon 19 deletion)-transfected MC-38.

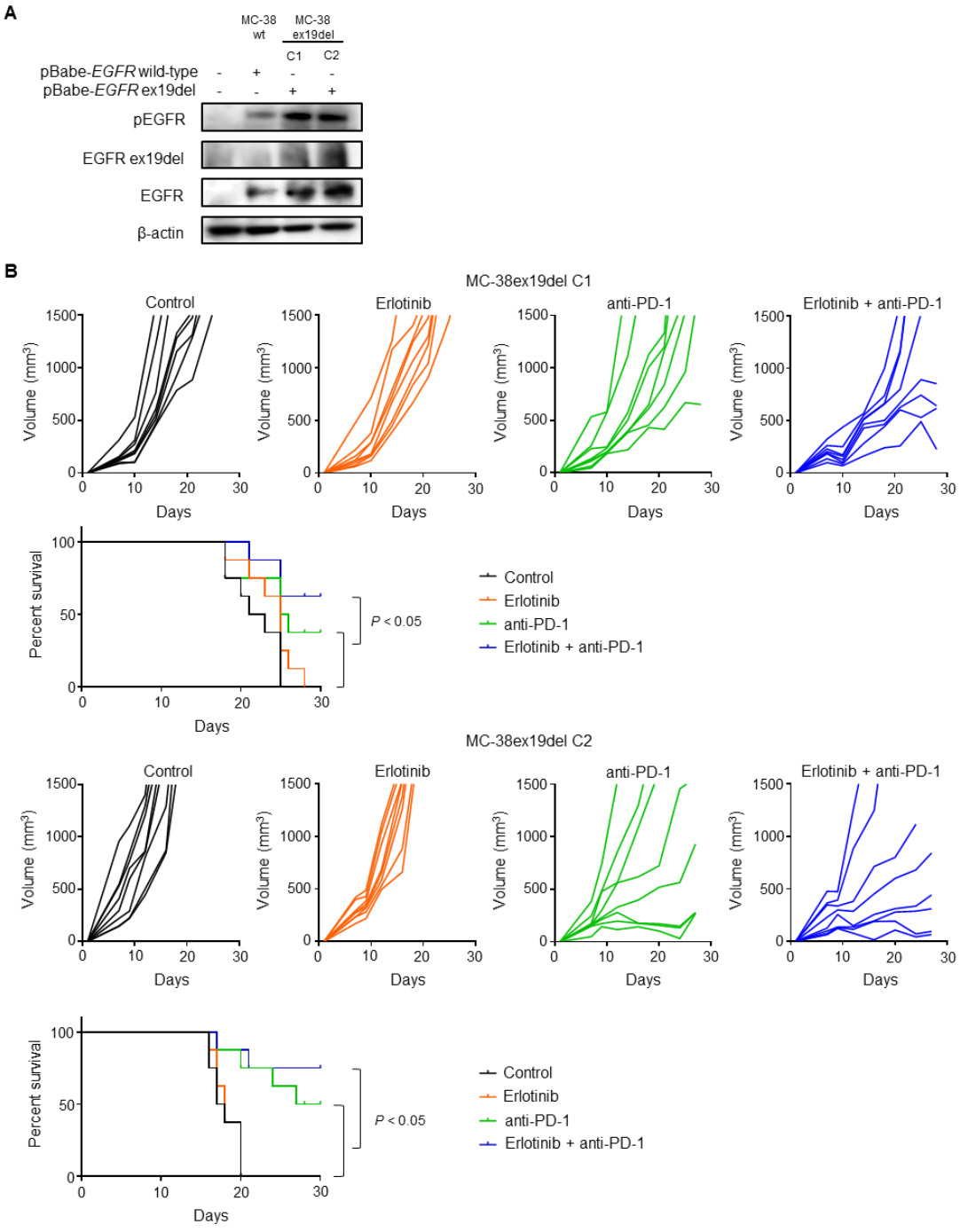

A. The human EGFR expression, phospho-EGFR, and exon 19-deleted EGFR of single clones of MC-38wt and MC-38ex19del were confirmed by western blotting of each clone.

B. Mice were inoculated with the single-cell clones of MC-38ex19del and treated with/without erlotinib, anti-PD-1 mAb or a combination (erlotinib + anti-PD-1 mAb). Tumor growth (top) and the survival curve (bottom) are shown. Representative data from two independent experiments are shown.

Fig. S13. *In vitro* proliferation and sensitivity to erlotinib in mock-transfected, wild-type and *EGFR* mutant (exon 19 deletion)-transfected MC-38 cell lines.

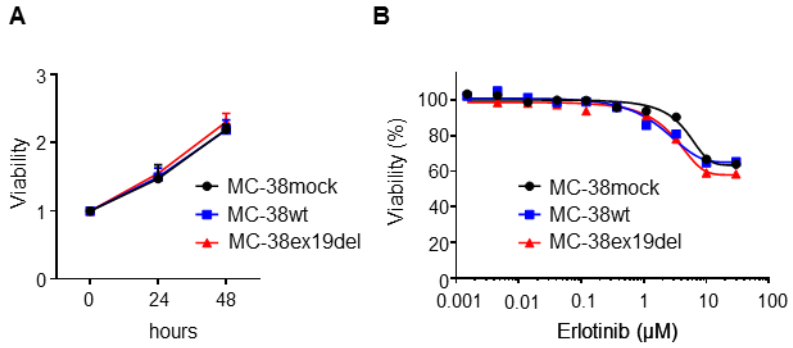

The proliferation of MC-38 mock, MC-38wt and MC38ex19del cells was analyzed 0, 24 and 48 hours after seeding with WST1 assays (**A**). Sensitivity to erlotinib was also analyzed 48 hours after erlotinib treatment with WST1 assays (**B**). Data are shown from three independent experiments. n.s., not significant.

Fig. S14. Changes in CD8$^+$ T cell and Treg infiltration in MC-39ex19del tumors following CXCL10 or CCL22 blockade administration, respectively.

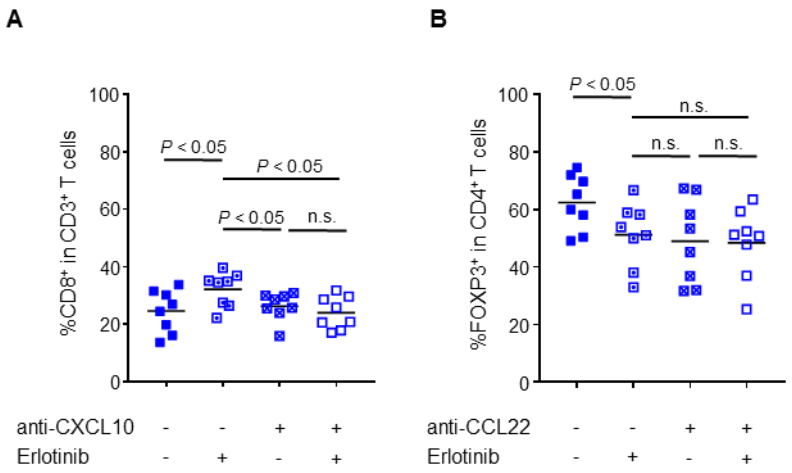

Mice were inoculated with MC-38wt or MC-38Ex19del and treated with/without erlotinib. For blocking CXCL10 and CCL22, 50 μg of anti-mouse CXCL10 mAb and 100 μg of anti-mouse CCL22 mAb, respectively, were administered intraperitoneally on days 4 and 8 after tumor cell inoculation. Tumors were collected on day 10, and tumor infiltrating CD8$^+$ T cells **(A)** and Treg**s (B)** were analyzed. Summaries of the frequency of CD8$^+$ T cells or Treg infiltration are shown. n.s., not significant.

Fig. S15. Antitumor effects by the combination of erlotinib and anti-PD-1 mAb in MC-38ex19del tumors under Treg-depleted conditions induced by anti-CD25 mAb.

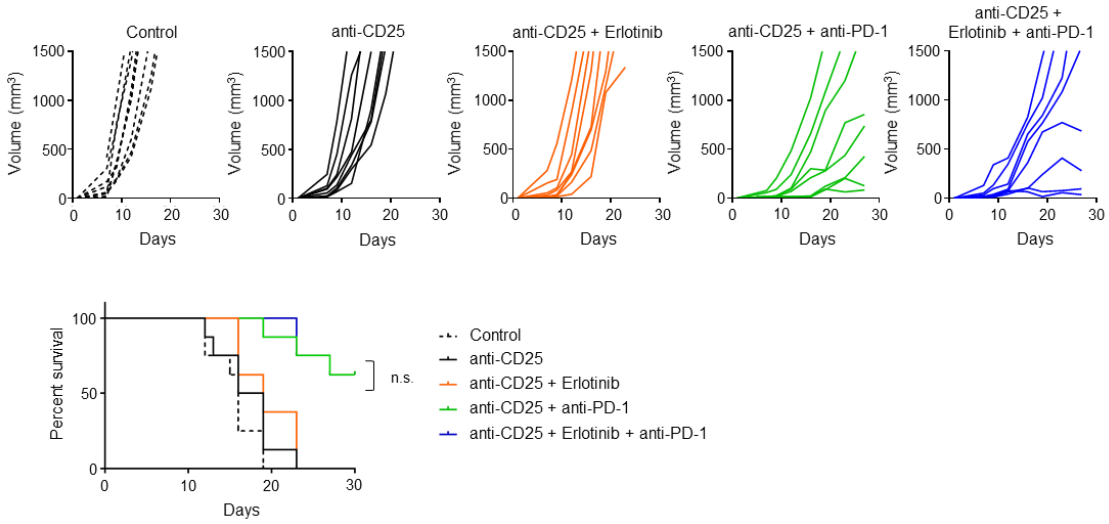

Mice were inoculated with MC-38ex19del and treated with/without erlotinib, anti-PD-1 mAb or the combination (erlotinib + anti-PD-1 mAb). For depletion of Tregs, 200 μg of anti-mouse CD25 mAb was administered intraperitoneally day 7 after tumor-cell inoculation. Tumor growth (top) and the survival curve (bottom) are shown. Representative data from two independent experiments are shown. n.s., not significant.

Fig. S16. The changes in other chemokines induced by EGFR signaling in microarray analysis.

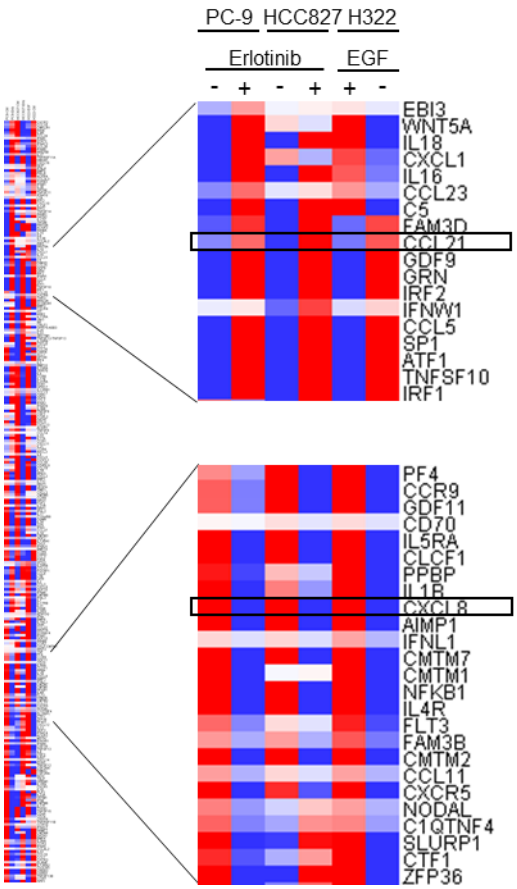

Two *EGFR*-mutated cell lines (PC-9 and HCC827) and an *EGFR* wild-type cell line (H322) treated with erlotinib and EGF, respectively, were subjected to microarray analysis. GO terms, cytokines and chemokines were examined.

Supplementary Tables

Table S1. Summary of LUADs patients who received surgery.

Features	*EGFR* gene status		*P*-value
	Mutation (8)	Wild-type (18)	
Age [Mean] (range)	67.4 years (42-80)	70.1 years (52-84)	0.58
Sex			
Male	4	16	0.051
Female	4	2	
Smoking status			
Never	4	5	0.38*
Past	4	10	
Current	0	3	
Stage			
I	4	10	0.63**
II	3	3	
IIIA	1	5	

*Never vs. past or current; **I or II vs. IIIA.

Table S2. Summary of LUAD patients who received EGFR-tyrosine kinase inhibitor therapy.

Features	N (11)
Age [Mean] (range)	67.2 years (46-82)
Sex	
Male	3
Female	8
Smoking status	
Never	7
Past	2
Current	2
Stage	
IIIB	1
IV	8
Recurrence after surgery or CRT	2
***EGFR* mutations**	
Exon 19 deletion	5
Exon 21 L858R	5
+T790M	1
Treatment line	
1st line	11
Regimen	
Gefitinib	7
Erlotinib	2
Afatinib	2
Sampling timing	
Pre-treatment	6
Post-treatment	5
Best response	
CR	1
PR	9
SD	0
PD	1

Table S3. Summary of antibodies used in the IHC.

Molecule	Clone	Company, catalog No., and ID
PD-L1	E1L3N	Cell signaling technology Cat#13684
CD8	C8/144B	Leica Biosystems Cat#NCL-CD8-4B11
FOXP3	SP97	Acris Cat#AM21067PU-N
CD33	EPR4423	Abcam Cat#ab134115
CD11b	EP1345Y	Abcam Cat#ab52478-100
CD11c	EP1347Y	Abcam Cat#ab52632-100
CD68	PG-M1	DAKO Cat#M087601-2
CD163	10D6	Leica Biosystems Cat#NCL-L-CD163
CD206	D-1	SantaCruz Cat#sc-376108
HLA-DR	TAL 1B5	Acris Cat#AM21067PU-N

Table S4. Summary of antibodies used in the CyTOF analyses

Tag	Molecule	Clone	Company and catalog No.
89Y	CD45	HI30	Fluidigm, Cat#3089003B
141Pr	T-bet	4B10	Fluidigm, Customized
142Nd	NFAT2	7A6	Fluidigm, Customized
143Nd	NFAT1	D43B1	Fluidigm, Cat#3143023A
145Nd	pZAP70	17a	Fluidigm, Customized
146Nd	CD8a	RPA-T8	Fluidigm, Cat#3146001B
147Sm	CD80	2D10.4	Fluidigm, Customized
148Nd	PD-L1	29E.2A3	Fluidigm, Cat#3148017B
149Sm	CCR7	4B17	Fluidigm, Customized
150Nd	Bcl2	N46-467	Fluidigm, Customized
151Eu	Eomes	WD1928	Fluidigm, Customized
152Sm	pAkt	D9E	Fluidigm, Customized
153Eu	CD45RA	HI100	Fluidigm, Cat#3153001B
154Sm	TIGIT	MBSA43	Fluidigm, Cat#3154016B
155Gd	PD-1	MIH4	Fluidigm, Customized
156Gd	CD86	IT2.2	Fluidigm, Cat#3156008B
158Gd	BATF	D7C5	Fluidigm, Customized
159Tb	FoxP3	256D/C7	Fluidigm, Cat#3159028A
160Gd	CD28	CD28.2	Fluidigm, Cat#3160003B
161Dy	CTLA-4	14D3	Fluidigm, Cat#3161004B
162Dy	CD69	FN50	Fluidigm, Cat#3162001B
163Dy	Bcl6	K11291	Fluidigm, Customized
164Dy	CD95 (FAS)	DX2	Fluidigm, Cat#3164008B
165Ho	LAG-3	11C3C65	Fluidigm, Cat#3165037B
166Er	pNFkB	S529	Fluidigm, Cat#3166006A
167Er	GATA3	TWAJ	Fluidigm, Customized
168Er	RORgT	B2D	Fluidigm, Customized

169Tm	CD25	2A3	Fluidigm, Cat#3169003B
170Er	CD3	UCHT1	Fluidigm, Cat#3170001B
171Yb	CD226	DX11	Fluidigm, Cat#3171013B
172Yb	Ki67	B56	Fluidigm, Cat#3172024B
173Yb	GrzB	GB11	Fluidigm, Customized
174Yb	CD4	SK3	Fluidigm, Cat#3174004B
175Lu	CCR4	L291H4	Fluidigm, Cat#3175035A
176Yb	pERK	D13.14.4E	Fluidigm, Customized
209Bi	cJun	2/c-Jun/(S63)	Fluidigm, Customized

Table S5. Summary of antibodies used in the flow cytometry analyses.

Tag	Molecule	Clone	Company and catalog No.
AF700	Human CD3	UCHT1	Thermo Fisher Science, Cat#56-0038-41
V500	Human CD4	RPA-T4	BD Biosciences, Cat#560769
BV785	Human CD8a	RPA-T8	BioLegend, Cat#301046
BV711	Human CD45RA	HI100	BD Biosciences, Cat#563733
PE	Human FOXP3	236A/E7	Thermo Fisher Science, Cat#72-5774-40
BV421	Human PD-1	MIH4	BD Biosciences, Cat#562516
BV421	Human EGFR	EGFR.1	BD Biosciences, Cat#563343
BV421	Human pSTAT5	pY694	BD Biosciences, Cat#562984
AF488	Human pJAK2	Phospho Y1007 + Y1008	Abcam, Cat#ab200339
AF700	Mouse CD3	17A2	Thermo Fisher Science, Cat#56-0032-80
V500	Mouse CD4	RM4-5	BioLegend, Cat#560782
BUV805	Mouse CD8	53-6.7	Thermo Fisher Science, Cat#564920
PE	Mouse FOXP3	FJK-16s	Thermo Fisher Science, Cat#12-5773-80
BV421	Mouse CD25	7D4	BD Biosciences, Cat#564571

Table S6. Primers used in qRT-PCR.

Symbol	Forward	Reverse
Human *CXCL10*	GAAATTATTCCTGCAAGCCAATTT	TCACCCTTCTTTTTCATTGTAGCA
Human *CCL5*	TTGCCTGTTTCTGCTTGCTC	TGTAACTGCTGCTGTGTGGT
Human *CCL22*	ATGGATCGCCTACAGACTGCACTC	CACGGCAGCAGACGCTGTCTTCCA
Human *JUN*	TTCTATGACGATGCCCTCAACGC	GCTCTGTTTCAGGATCTTGGGGTTAC
Human *IRF1*	CCTGATACCTTCTCTGATGGACTCA	GCTCTGTTTCAGGATCTTGGGGTTAC
Mouse *CXCL10*	CCAAGTGCTGCCGTCATTTT	TTCAAGCTTCCCTATGGCCC
Mouse *CCL5*	TGCAGAGGACTCTGAGACAGC	GAGTGGTGTCCGAGCCATA
Mouse *CCL22*	TCTTGCTGTGGCAATTCAGA	GCAGAGGGTGACGGATGTAG
Mouse *JUN*	GTTGCGGCCGCGAAACTT	CATTGCCCTCGAGCCCTG
Mouse *IRF1*	CCTGGGTCAGGACTTGGATA	TTCGGCTATCTTCCCTTCCT

Table S7. Summary of antibodies used in western blotting.

Molecule	Clone	Antibody	Company, catalog No., and ID
cJun	60A8	Rabbit monoclonal antibody	Cell signaling technology Cat#9165
Phospho-cJun	54B3	Rabbit monoclonal antibody	Cell signaling technology Cat#2361
JNK	Polyclone	Rabbit polyclonal antibody	Cell signaling technology Cat#9252
Phospho-JNK	Polyclone	Rabbit polyclonal antibody	Cell signaling technology Cat#9251
AKT	Polyclone	Rabbit polyclonal antibody	Cell signaling technology Cat#9272
Phospho-AKT	D9E	Rabbit monoclonal antibody	Cell signaling technology Cat#4060
NF-κB	D14E12	Rabbit monoclonal antibody	Cell signaling technology Cat#8242
Phospho-NF-κB	93H1	Rabbit monoclonal antibody	Cell signaling technology Cat#3033
EGFR	D38B1	Rabbit monoclonal antibody	Cell signaling technology Cat#4267
Phospho-EGFR	Polyclone	Rabbit polyclonal antibody	Cell signaling technology Cat#2234
EGFR (E746-A750del)	D6B6	Rabbit monoclonal antibody	Cell signaling technology Cat#2085
IRF1	C-20	Rabbit polyclonal antibody	SantaCruz Cat#sc-497
β-actin	13E5	Rabbit monoclonal antibody	Cell signaling technology Cat#4970